Hyperspectral image analysis of Aguas Teñidas, Magdalena, Sotiel and Majada deposits: towards a drill-core scan in the Iberian Pyrite Belt

Pedro S.T. Mendes, Pierre Barnabé, Eric Pirard
Minerals Engineering, Materials and Environment (GeMMe), Université de Liège, Belgium

Juan Manuel Pons, Juan Carlos V. Vasquez
Minas de Aguas Teñidas SAU (MATSA), Spain

Carlos G. Piña
DMT GmbH & Co. KG

Abstract. Analysis of VNIR-SWIR hyperspectral images is presented to assist the development of a multi-sensor scanning system for Iberian Pyrite Belt Cu-Zn-Pb projects. Fisher Linear Discriminant and Linear Support Vector Classifier were used for supervised classification after pre-processing, spectral plotting and construction of false color composites. Validation is given by mean accuracy of confusion matrices for different scenarios considering parameters of practical applications in industrial settings. Interpretation indicates a different performance for shale and volcanic-hosted deposits. The results demonstrate the power of machine learning algorithms and hyperspectral databases applied to an automated technique to assist the traditional logging. Combined to other sensors, the methodology should be adapted to a drill-core scan delivering cost-effective and time-saving outcomes.

1 Introduction

Hyperspectral imaging (HSI) concentrates on the diversity of spectral properties inherent to each material. In other words, the light that is emitted or reflected and its variation along narrow wavelength ranges. The link between these physical properties and earth sciences has emerged to map geological parameter in different scales (Hunt 1977; Goetz et al. 1985).

The logging of drill cores has been carried out by geologists using visual inspection. Despite providing important basic information, the technique has demonstrated to be subjective. In this work, the potential of machine learning algorithms combined to HSI is evaluated as an automated logging tool by testing different supervised classification strategies. The chosen method is considered supervised because it is assisted by a previous user knowledge (Han et al. 2012).

This research aims to contribute to the classification of rocks in the Iberian Pyrite Belt volcano-sedimentary complex in a consistent manner. The work comprises a fundamental step of ANCORELOG, an EIT Raw Materials-funded project working on the development of a multi-sensor analytical drill-core scan. Finally, the new prototype will extend the functionality of DMT CoreScan System, improving utilization of ore bodies from exploration to mineral processing (Lamberg 2012).

Predictions of performance in practical applications are evaluated for the following Cu-Zn-Pb ventures: Aguas Teñidas and Patata Frita (ATE); Magdalena (MAG); Sotiel and Elvira (SOT); also, the drilling campaign of Majada (MAD). The underground mines and surface exploration areas associated to each deposit are illustrated in Fig. 1.

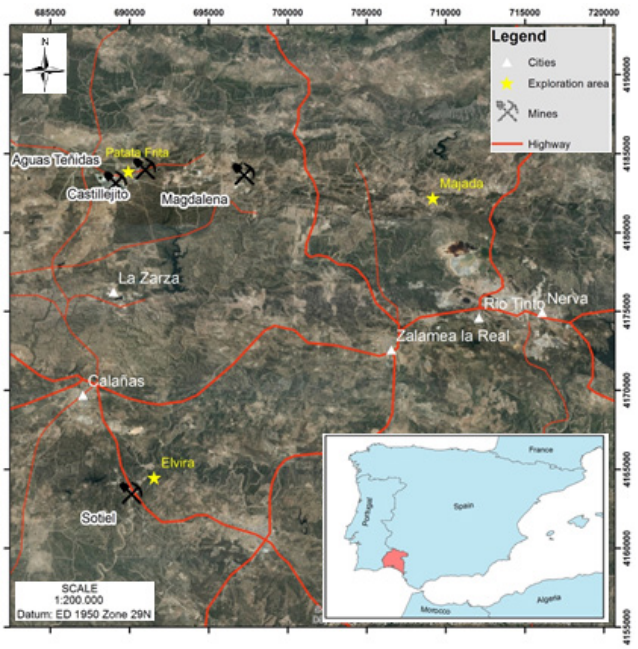

Figure 1. Study area (Mendes 2018).

2 Methodology

2.1 Sampling

Characterization was carried out through visual drill core logging and mine front description. The divergence between two metallonegetic environments was considered (Martin-Izard et al. 2016): Shale hosted deposits of Type 1 (SOT and MAD) and Volcanogenic Massive Sulphides (VMS) of Type 2 (ATE and MAG), where extrusives dominate.

In total 40 samples were collected following a systematic protocol to ensure representativeness of lithology, texture, alteration degree and metal grade.

Chemical assays of valuable metals and penalty elements from 10 mineralized samples with cupriferous stockwork and massive cupriferous/polymetallic ore were given by ICP-OES. Main minerals are chalcopyrite, sphalerite and galena.

2.2 Image acquisition and pre-processing

The images were acquired using a Specim SWIR camera and a VNIR, which is composed by a Specim ImSpectorV10E spectrograph and a Photonfocus MV1-D1312ie sensor (Fig. 2). Both cameras are placed horizontally over a 2.5 m frame to detect the reflected light from the samples in a line pointing the conveyor belt through mirrors (Barnabé et al. 2015). The approximately 350 mm line in the field of view is placed at the focuses of extruded elliptical reflectors so it is illuminated with constant light by halogen lamps, that are situated at the other focuses.

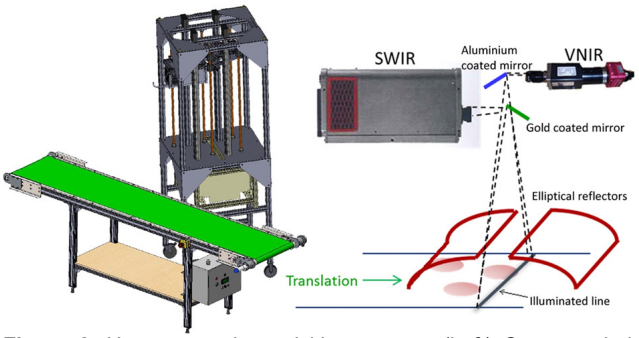

Figure 2. Hyperspectral acquisition system. (Left) Conveyor belt and metallic frame. (Right) VNIR and SWIR cameras, mirrors and illumination system with halogen lamps and extruded elliptical reflectors (Barnabé et al. 2015).

By combining data from two sensors, the result image is composed by 323 bands of 6.25 nm and digital pixels of approximately 0.25 mm². Images were spatially cropped to keep only regions of interest, avoiding long computational time. Bands up to 500 nm were considered noisy due to the high variation of pixel intensity within the spectra, which masks mineral overtones. This wavelength range was therefore removed to avoid algorithm's confusion regarding true classifications.

2.3 Spectral response

The mean spectrum of each sample was extracted from a random 20 x 20 - pixel window and plotted in a reflectance versus wavelength chart. This procedure along with False Color Composites (FCC) assisted interpretation of classification challenges to segregate rocks with similar spectral response.

Three bands were extracted from the SWIR database to highlight the presence of alteration minerals with deep absorption in the spectra. The 1940, 2200 and 2340 nm ranges were associated to the bands of an RGB image (Table 1), where reflectance is attenuated due to the presence of water, white mica and carbonate / chlorite / amphibole / white mica, respectively.

Since pixel intensity decreases in a specific wavelength interval when absorption occurs, the output represents relative concentrations where the target minerals are displayed by colors related to the opposite bands. White micas are normally concentrated in red-pinkish regions, water-rich material is represented by blue pixels and green areas are linked to carbonate / chlorite / amphibole / white mica occurrences and to the wooden box (GTK 2018 unpublished presentation). Finally, saturation and contrast were enhanced to intensify local color transitions.

Table 1. RGB bands associated to SWIR absorptions due to mineral assemblages.

RGB Band	Short Wave Infrared (nm)	Chemical group	Mineral Assemblage
R	1940	H_2O	Water
G	2200	AlOH	White Mica
B	2340	MgOH and CO_3	Carbonate/Chlorite/ Amphibole/White Mica

2.4 Supervised classification

Supervised classification was undertaken using machine learning algorithms in the perClass Library for Matlab (Fig. 3). The objective of supervised classification is to assign an image pixel to a known lithology. Dimensionality reduction with Principle Component Analysis (PCA) indicated a fall of overall performance and was initially rejected. The algorithms able to handle the dataset with satisfactory accuracy for convenient interpretation were selected: Fisher Linear Discriminant and Linear Support Vector Classifier (LSVC) (Table 2).

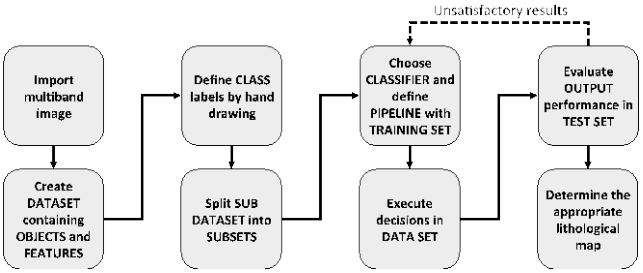

Figure 3. Scheme of supervised classification (Mendes 2018).

Table 2. Algorithms for supervised classification (Mendes 2018).

Classifier	General description
Fisher Linear Discriminant	Composed by a Linear Discrimination Analysis (LDA) component followed by a Gaussian Model
Linear Support Vector Classifier	It finds the hyperplane that separates data by classes after transforming the training set into a higher dimension.

A total of 41 classes (samples + box) are combined to test two different strategies: First, VNIR and SWIR ranges are cropped from the dataset to evaluate the performance of cameras together and individually. Subsequently, the size of training set is modified to identify the sensitiveness of classification regarding the number of labelled pixels.

The approach represents the variation of scenarios ruled by accuracy and costs.

Accuracy is computed by the mean error over classes from a confusion matrix which shows the relationship between true labels and classifier decisions.

3 Results

In general, fault rocks and bright volcanics such as dacites, breccias and tuffites show similar profile due to the presence of water and OH-bearing molecules whereas calcite veins emphasize the very deep absorptions at 2340 nm (Fig. 4). The exceptions are rocks with strong silicification such as a few tuffs and the black rhyolite. Sulphides and shales display flat curves.

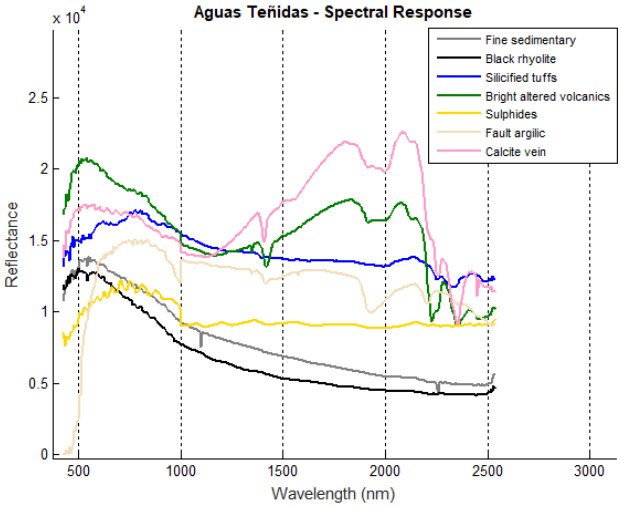

Figure 4. Spectral response of Aguas Teñidas rocks (Modified from Mendes 2018).

False Color Composites (Fig. 5) emphasize the difference between deposits of Type 1 (MAD and SOT) and Type 2 (ATE and MAG). While the latter display colourful regions, most of Type 1 samples contain dark pixels due to shales and massive/stockwork sulphides with lack of absorption features. Usually, volcanics have pink to greenish matrix where alumino-phyllosilicate-bearing zones are either intercalated or cut by thin veins of chlorite. The brightest green sample is the calcite vein located in the upper-right corner of ATE 2.

In addition, ATE 2 samples confirm an association of metal content and alteration aureoles in the Cu stockwork area of the deposit. As the segments move outwards from the mineralized zone, grey and greenish pixels are substituted by pink and reddish matrices. The network of thin veins of chalcopyrite immersed in a chloritic matrix decreases as the volume of barren sericite-rich material increases together with fine disseminated pyrite.

The supervised classification using both cameras and LSVC is the most consistent overall (Fig. 6). Average accuracy is close to 100% if LSVC is combined to many spectral bands. When only the SWIR data is used both algorithms show a slight increase in classification error. The incapability of LSVC of dealing within a small feature space is evident when only the VNIR camera is selected (78 bands). The algorithm loses almost entirely its capability of classification.

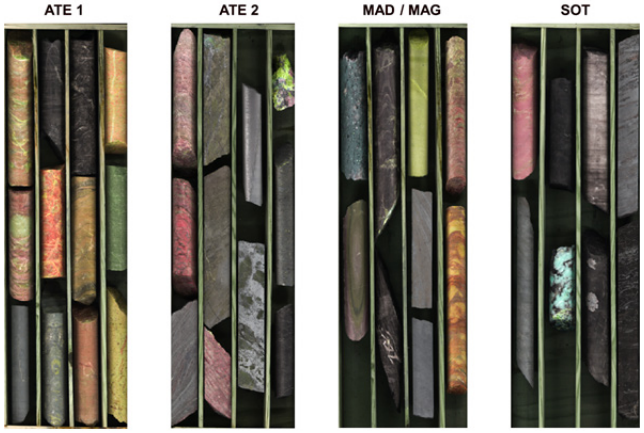

Figure 5. False color composites for alteration minerals. MAD and SOT are included in Type 1 whereas ATE and MAG are Type 2.

Another drawback of LSVC is time. The algorithm runs at low speed in most of the cases whereas decision time for Fisher is practically negligible in every scenario. Even though the accuracy of Fisher drops from almost 100% to 80% when only VNIR is used, the interpretation of images is still possible in this situation. In the case of SWIR by itself, time is the crucial parameter to elect Fisher as the best option.

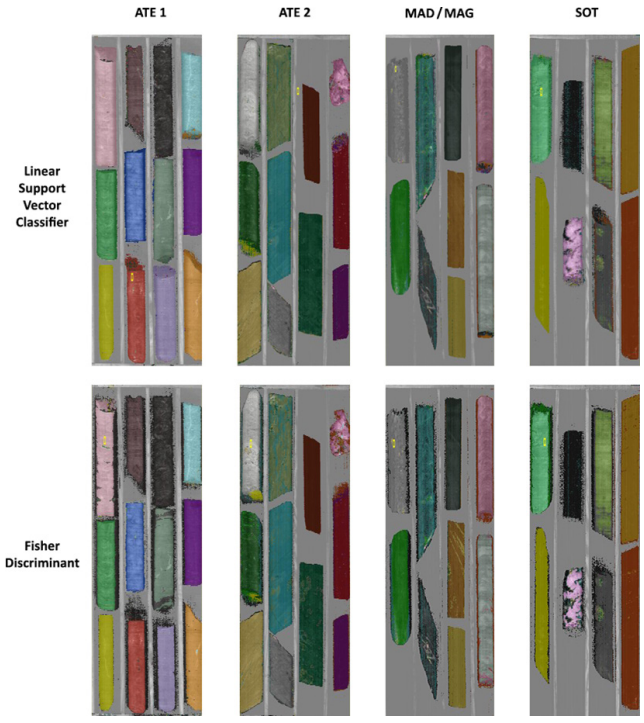

Figure 6. Most accurate classification scenario overall: VNIR-SWIR database, large training size and 41 class labels. LSVC performance is slightly more accentuated in this case. Accuracy for both type of deposits is close to 100% so that a comparison of misclassified pixels between them can be hardly evaluated through classified images (Mendes 2018).

Overall sensitiveness against training set for both classifiers is similar. However, Fisher is less accurate than LSVC at very limited subset fractions. Bearing in mind that some classes in the smallest training set (Tr4) are represented by around 5 pixels out of a test set containing 3 million pixels, the consistency of LSVC can be considered outstanding in terms of accuracy and image interpretation if applied to practical logging applications (Fig. 7).

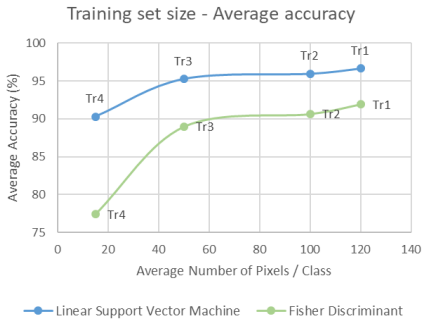

Figure 7. Accuracy with varying training set sizes (Mendes 2018).

Performance reflects the variation of absorption features in the spectra profile, being more consistent for volcanics than fine clastics in every tested scenario of classification as seen in Fig. 8.

Figure 8. – Accuracy for the two deposit types (Mendes 2018).

4 Discussion

FCC and supervised classification reveal the ability of HSI to discriminate alteration degrees and rock types (Schneider et al. 2014). However, algorithms are dependent on investment in cameras and hardware.

Results demonstrate that reflectance and depth of absorption is extremely affected by grain size. Coarse material absorbs more radiation penetrating to the surface than fine grain size. The optical path is explained by the Labert-Beer Law (Zaini et al. 2012).

Since the diversity of lithologies increase in projects within time, the capability of both algorithms to deal with many classes is an advantage. Fisher is preferable over LSVC when time is crucial and when dealing with cameras independently. A significant increase in training set size can improve Fisher performance without compromising computational effort.

Areas at early exploration stages should consider a robust training set with a large number of classes from different parts of the IPB. On the other hand, drill holes from mine sites can count on a training set with restrict number of classes with only the known local lithologies.

5 Conclusion

A real performance can only be evaluated when applying decisions to complete drill cores on site. It should adapt the methodology to real geological sections where transitional contacts and textural variations are impractical to be sampled in a representative manner.

The analysis of spectral profiles with the support of FCC assists the re-construction of unbiased labels to define new logging classes. Automatization using HSI and machine learning can therefore simplify 3D models in the IPB. It can also save time and costs in projects where exploration rushes to find new deposits and to characterize the ore constantly feeding the plant.

This study successfully meets the first steps of ANCORELOG with promising business opportunities when applied to end-users such as mining companies and research institutes.

Future works should improve pixel-wise segmentation. Grades will be included through the fusion of HSI with the output of other sensors such as RGB camera, X-Ray Fluorescence (XRF), Laser Induced Breakdown Spectroscopy (LIBS) and time-gated Raman spectroscopy.

Acknowledgements

The authors would like to thank the involved team from MATSA and GeMMe for the constant support. Also, ANCORELOG partners, EMerald and EIT Raw Materials for the effort in education and research.

References

Barnabé P, Dislaire G, Leroy S, Pirard E (2015) Design and calibration of a two-camera (visible to near-infrared and short-wave infrared) hyperspectral acquisition system for the characterization of metallic alloys from the recycling industry. J Electronic Imaging 24: 61115.

Goetz, AFH, Vane G, Solomon JE, Rock BN (1985) Imaging Spectrometry for Earth Remote Sens Science 228:1147–1153.

Han J, Kamber M, Pei J (2012) Data Mining: Concepts and Techniques. Morgan Kaufmann, San Francisco

Hunt GR (1977) Spectral Signatures of Particulate Minerals in the Visible and Near Infrared. Geophysics.

Lamberg P (2012) Geometallurgy–new/old methodology to improve resource management. Materia 70:52-55.

Martin-Izard A, Arias D, Arias M, Gumiel P, Sanderson DJ, Castañon C, Sanchez J (2016) Ore deposit types and tectonic evolution of the Iberian Pyrite Belt: From transtensional basins and magmatism to transpression and inversion tectonics. Ore Geology Rev 79:254–267.

Mendes, PST (2018) Multi-sensor analysis of Aguas Teñidas, Magadalena, Sotiel and Majada deposits, Iberian Pyrite Belt, Spain: Analytical drill core-scanning for optimized exploration of ore. Dissertation, University of Liege.

Schneider S, Murphy RJ, Melkumyan A (2014) Evaluating the performance of a new classifier - the GP-OAD: A comparison with existing methods for classifying rock type and mineralogy from hyperspectral imagery. ISPRS J Photogrammetry and Remote Sens 98:145–156.

Zaini N, Van der Meer F, Van der Werff H (2012) Effect of grain size and mineral mixing on carbonate absorption features in the SWIR and TIR wavelength regions. Remote Sens 4:987-1003

High-resolution short-wave infrared hyperspectral characterisation of alteration at the Sadiola Hill gold deposit, Mali, Western Africa

Semyon Martynenko, Pekka Tuisku
Oulu Mining School, University of Oulu, Finland

Frank J.A. van Ruitenbeek
Faculty of Geo-Information Science and Earth Observation (ITC), Netherlands

Kim A.A. Hein
School of Geosciences, University of Witwatersrand, South Africa

Abstract. Sadiola Hill is an ~8 Moz gold deposit located in western Mali within a ca. 2200-2050 Ma tectonic window known as Kédougou-Kénieba inlier (KKI), exposing the Western African craton. The deposit is hosted in a metasedimentary package made up of impure carbonate rocks, wackes, and arenites intruded by three distinct igneous phases. A N-S-trending Sadiola shear zone, related to the regional Senegal-Mali shear zone, and NNE-trending third order fault splays acted as conduits for auriferous hydrothermal fluid flow. The deposit has undergone a complex poly-phase alteration history. Alteration assemblages related to gold mineralization consist of biotite-carbonate-quartz-sulphide. Other assemblages include calc-silicates, chlorite, white mica, scapolite, and tourmaline (Hein and Tshibubudze 2007; Cameron 2010; Masurel et al. 2017). Current research is aimed at characterising alteration at the mineral-scale, as well as assessment of cooling trend(s) and alteration footprint(s) with high-resolution short-wave infrared (SWIR) hyperspectral scanning. In addition to detailed mineralogical classification, changes in fluid chemical parameters are determined with variations in white mica, namely, the position of Al-OH bond in the SWIR range and white mica crystallinity. Furthermore, hydrothermal fluid chemistry is assessed with Fe^{2+} content in carbonate group minerals**.** Protolith control on alteration expression is also investigated.

1 Introduction

Short-wave infrared (SWIR) hyperspectral imaging is a rapid and reliable technique for mineral identification. It has proven reliable at tracing hydrothermal fluid pathways in diverse range of deposit types, including orogenic gold systems in granite-greenstone terranes (van Ruitenbeek et al. 2012; Wang et al. 2017). In addition to precise identification of phyllosilicates and carbonates, SWIR spectroscopy identifies specific mineral parameters, such as Al-Si substitution in white mica, that correspond to physico-chemical changes of hydrothermal fluid (van Ruitenbeek et al. 2005). As such, it has become an effective vectoring tool in mineral exploration (Wang et al. 2017; Roache et al. 2011).

Current research investigates alteration assemblages within a world class Sadiola Hill gold deposit with SWIR hyperspectral imaging and conventional petrography. The study establishes paragenetic sequence and the number of hydrothermal events within the system. Spatial variation in the chemical composition of alteration minerals, and protolith control on alteration expression are also determined. The research is carried out on drill core samples from 6 diamond holes capturing the most representative alteration examples and is solely laboratory based. The core samples are scanned at medium (0.26mm pixel size) and high-resolution (26µm pixel size) scales. Paragenetic context of aspectral alteration mineralogy is determined with transmitted light microscopy. Spectral classes of the 26µm-pixel mineral maps are validated with petrographic observations and electron microprobe analyses.

2 Geologic setting

The West African craton exposed in the Kédougou-Kénieba inlier (KKI) is a unique Paleoproterozoic granite-greenstone belt as it contains a package of carbonate rocks of variable thickness not typical for other granite-greenstone belts worldwide. The KKI is comprised of series of volcano-plutonic belts and sedimentary basins dissected by two major regional faults, namely, the Main Transcurrent Zone (MTZ) and the Senegal-Mali Shear Zone (SMSZ). (Hein et al. 2015; Masurel et al. 2016).

Previous studies have revealed that Sadiola impure carbonates are overlain by a package of greywacke. Impure carbonates and detrital sediments have been intruded by three intrusive suites: early diorite, quartz feldspar porphyry, and late diorite. The rocks have undergone a regional mid-greenschist facies metamorphism (Hein and Tshibubudze 2007; Masurel et al. 2017).

Sadiola Hill records a complex brittle-ductile history evident from 3 distinct pre- and syn-mineralization deformation events as well as two smaller scale brittle events postdating gold deposition (Masurel et al. 2017). The key structural features of the Sadiola Hill deposit include the N-S-trending subvertical to vertical Sadiola shear zone, and associated NNE-trending fault splays. The Sadiola shear zone marks the major structural break

at Sadiola separating greywackes on the western side of the pit from marbles on the eastern side (Hein, 2008). Most notable is the D_3 deformation event that resulted in sinistral reactivation of Sadiola shear zone and the NNE-trending splays and was syn-genetic to auriferous hydrothermal fluid flow along these structures (Hein and Tshibubudze 2007; Cameron 2010; Masurel et al. 2017).

Complex poly-phase alteration history at Sadiola Hill consists of ore stage K-feldspar-biotite-carbonate-quartz-sulphide potassic alteration assemblages. Other assemblages include calc-silicates related to contact metamorphism during emplacement of igneous suits into the sedimentary package, as well as chlorite, white mica, scapolite, and tourmaline (Hein and Tshibubudze 2007; Cameron 2010; Masurel et al. 2017).

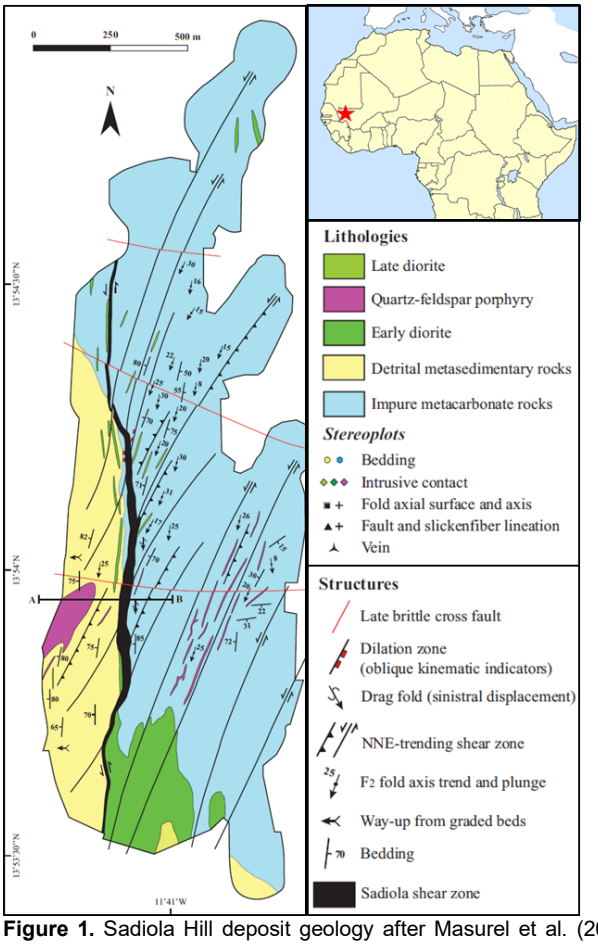

Figure 1. Sadiola Hill deposit geology after Masurel et al. (2017) Inset map shows deposit's location near Senegal-Mali border in Western Africa.

3 SWIR hyperspectral imaging

3.1 Background

SWIR hyperspectral imaging uses light reflection is 1000nm-2500nm range of the electromagnetic spectrum. Cation-OH, H_2O, $(CO_3)^{2-}$ in crystal structures reflect light in characteristic way producing diagnostic absorption features in the SWIR range (Clark 1999). White mica is characterized by absorption features positioned at 2200nm related to Al-OH bond, and 1900nm absorption feature corresponding to H-OH bond. Tschermak substitution of Al^{3+} by Fe^{2+} and Mg^{2+} in muscovite crystal structure shifts position of Al-OH bond to longer wavelength (Dalm et al. 2017). Illite spectral response shows a subtle difference from white mica responses, as illite also has a deep absorption feature around 2200nm related to Al-OH bond as well as OH and H-OH bonds at 1400nm and 1900nm respectively (Agus 2011; Clark 1999).

Actinolite-tremolite series are distinguished by hydroxyl stretching and bending vibrations located near 2320nm and 2390nm as well as ferrous drop (Laukamp et al. 2012). Epidote-clinozoisite series distinguished from chlorites by 1550nm absorption feature. Spectral responses of chlorite are attributed Mg-OH and Fe-OH bonds at ~2340nm and ~2250nm respectively that shift to longer wavelengths with Fe^{2+} substituting for Mg^{2+}. Carbonate group minerals (Figure 2) are identified by $(CO_3)^{2-}$ absorption band between 2300 and 2360nm combined with ferrous drop related to Fe^{2+} substitution into crystal structure (Clark 1999; Roache et al. 2011).

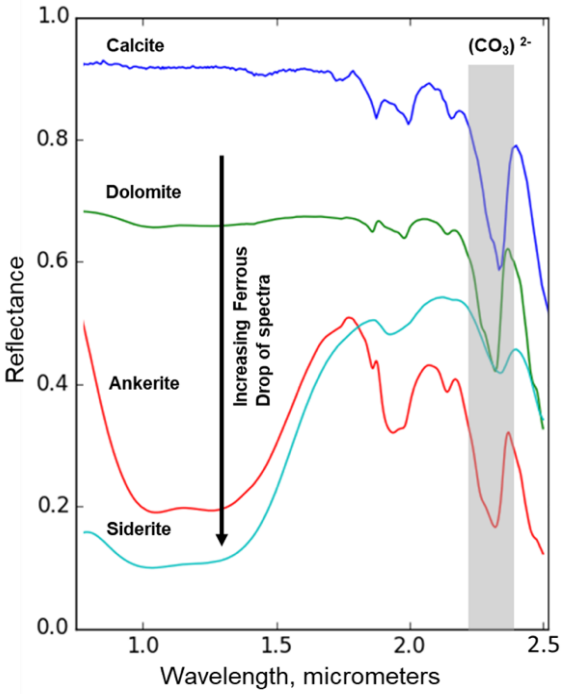

Figure 2. Spectral responses of carbonate group minerals in the SWIR range. Note ferrous drop in siderite and ankerite spectra. Figure generated from USGS spectral library version 7 after Kokaly et al. (2017).

3.2 Methodology

Hyperspectral scanning of drill core samples and offcut blocks was acquired at Faculty of Geo-Information Science and Earth Observation (ITC), University of Twente with Specim Hyperspectral camera at medium (0.26mm pixel size) and high-resolution (26µm pixel size). Data for each pixel is collected in x-, y-, and z-direction with x- and y-values of the pixel cube corresponding to length and width of a pixel within a horizontally stationed sample. Z-values represent a stack

of bands in the SWIR range with 12 nm spectral resolution, amounting for the total of 288 bands. Conversion of the raw data into calibrated hyperspectral images was done with hyperspectral python (hyppy), an in-house software developed in ITC. Calibrated images were converted into wavelength maps over 6 different ranges capturing depth and position of 1st, 2nd, and 3rd deepest absorption features. Decision trees are developed for project-specific mineralogy as matching algorithms between recorded bands to spectra from USGS spectral library. Polished thin sections were prepared from drill core samples scanned at high-resolution for one-to-one comparison of mineral maps to petrographic observations (van Ruitenbeek et al. 2017). Conventional transmitted light microscopy is added to the workflow to validate hyperspectral mineral maps and to add paragenetic constraints related to cross-cutting relationships and replacement textures to the interpretation. Exact stoichiometry of each spectral class is determined with electron microprobe.

Decision tree for muscovite and illite was constructed from combination of illite crystallinity, a ratio of depth of Al-OH absorption feature to the depth of water feature, and position of Al-OH bond. Overall, crystallinity was divided into 4 classes (>1, >2, >3, >4) based on observed variability in the samples. Position of Al-OH bond was assessed with 5nm breaks within Al-OH feature range.

Decision tree for carbonate group minerals has been developed based on Fe^{2+} drop values and presence of $(CO_3)^{2-}$ absorption feature. Secondary Fe-OH feature near 2250nm was applied to filter out Fe-bearing phyllosilicates and epidote from carbonate classification. Position of the carbonate feature for ankerite, dolomite, and calcite were taken from the USGS spectral library and related studies (Kokaly et al. 2017).

Decision tree for classification of chlorites, calcic amphiboles, epidote and tourmaline was developed from combination of wavelength positions of the 1st and 2nd deepest absorption features in the 2100-2400nm range combined with position of the deepest features in 1850-2100nm and 1300-1600nm ranges. Ferrous drop was also utilized for tremolite-actinolite classification.

4 Preliminary results

Muscovite is more aluminous in igneous units in comparison to greywacke and impure carbonate reflecting availability of Al^{3+}. In cases where Na^{+} is ubiquitous, e.g. tonalite unit, white mica composition changes to paragonite (Figure 3). Mineral-scale variations were also noted in muscovite. When muscovite replaces biotite, Al-OH feature shifts to longer wavelengths (~2210nm) consistent with incorporation of Mg^{2+} from biotite into muscovite crystal structure. Illite crystallinity has a common trend of increasing inward into a vein and is also protolith dependent, with low crystallinity illites constrained to greywacke and muscovite to igneous units and impure carbonates.

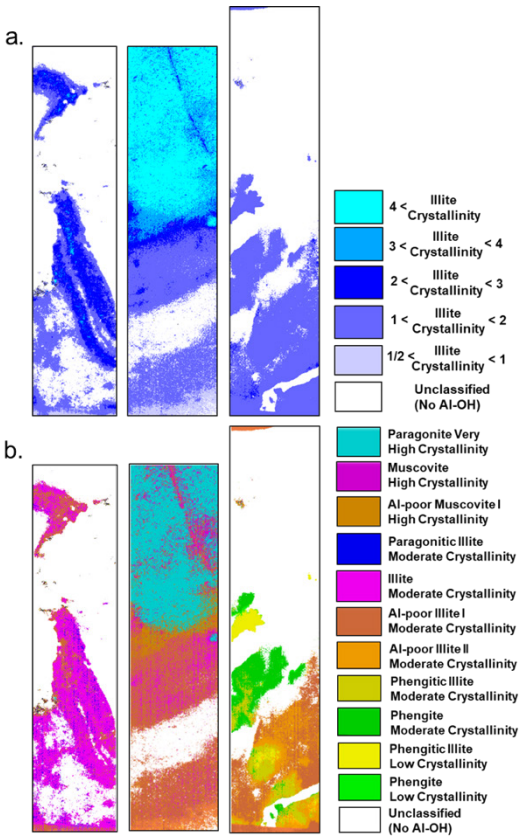

Figure 3. a. Illite crystallinity maps and **b.** corresponding illite/muscovite mineral maps of impure carbonate unit (left), tonalite-greywacke contact (centre), and greywacke (right) showing compositional variation in white mica. Map width is 10mm.

Ore-stage vein-controlled and pervasive carbonate alteration is represented by ferroan dolomite and ankerite in greywacke and diorite. Hyperspectral imaging of the least altered and umineralized samples of impure carbonate unit revealed it is dolomite-calcite dominant. In contrast, calcite is absent in the ore-zone impure carbonate samples. Hydrothermal calcite reoccurs in the system as late post-mineralization fracture-fill phase (Figure 4).

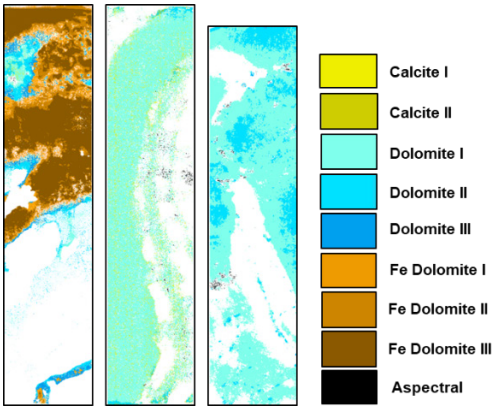

Figure 4. Carbonate mineral maps at 26µm pixel resolution showing variation and complexity of Sadiola Hill carbonate mineralogy. Ferroan dolomite vein cutting greywacke (left), least-altered (centre) and ore-zone (right) dolomite-calcite impure carbonate. Map width is 10mm.

Overall, alteration mineralogy at Sadiola Hill is variable and strongly protolith-dependent evident from both white mica and carbonate chemistry. Reactive folded argillaceous laminae within the impure carbonate acted as chemical trap for gold mineralization during the D_3 event. Biotite supplied iron for sulphidation reactions leading to pyrrhotite- arsenopyrite- chalcopyrite-sphalerite- pyrite- free gold precipitation (Figure 5). Dolomite-dominant laminae do not host sulphide-gold mineralization, but track CO_2 addition from auriferous fluid to impure carbonate host. Mineralization within greywacke is more sporadic with iron also sourced from biotite and is associated with patchy ferroan dolomite alteration, reflecting decomposition of silicates. Phlogopite occurs in all lithologic units in association with sulphides consistent with transition to Mg-rich silicate phase in response to iron consumption by sulphidation reactions.

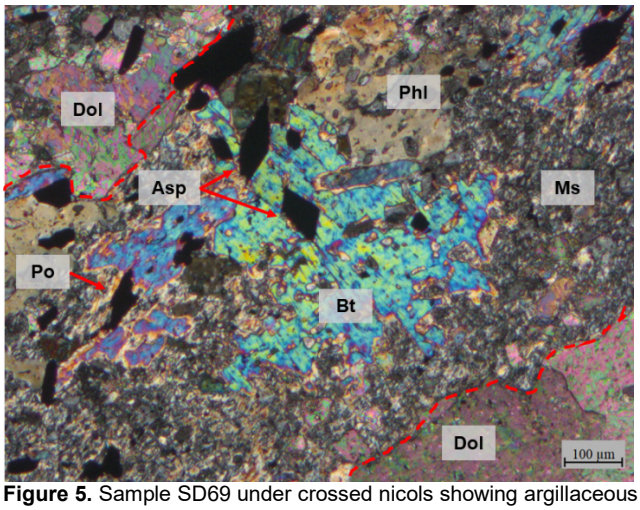

Figure 5. Sample SD69 under crossed nicols showing argillaceous layer (outlined by dashed red line) within dolomitic impure carbonate unit. Note biotite-phlogopite-sulphide associations and fine-grained muscovite-dolomite aggregates. Abbreviations: Asp = arsenopyrite; Bt = biotite; Dol = dolomite; Ms = muscovite; Phl = phlogopite; Po = pyrrhotite.

5 Future work

Zonation of ore-stage carbonate group minerals and chemical variations of white mica proximal and distal to ore will be investigated further. Cross-cutting relationships and chemical composition of carbonates will be assessed with cathodoluminescence (CL). Furthermore, drill core samples scanned at 26µm resolution have been submitted for complete geochemical characterization to ALS Global (results pending). Trace element associations will compliment hyperspectral interpretation of the alteration footprint and cooling trends within the system. In addition, protolith control on mineralization and alteration expression will be further constrained.

Acknowledgements

Dr. Asinne Tshibubudze, School of Geosciences, University of Witwatersrand, is thanked for arranging funds for geochemical analyses for this project.

References

Agus JL (2011) Mapping White Mica in Milled Prophyry Copper Pebbles Using Hyperspectral Imagery: An Exploration Study. MSc. Thesis Report. Faculty of Geo-Information Science and Earth Observation. University of Twente.

Clark RN (1999) Chapter 1: Spectroscopy of Rocks and Minerals, and Principles of Spectroscopy. Manual of Remote Sensing. Remote Sensing for the Earth Sciences 3:3-58.

Dalm M, Buxton MWN, van Ruitenbeek FJA (2017) Discriminating ore and waste in a porphyry copper deposit using short-wave infrared (SWIR) hyperspectral imagery. Mineral Engineering 105:10-18.

Laukamp C, Termin KA, Pejcic B, Haest M, Cudahy T (2012) Vibrational spectroscopy of calcic amphiboles - applications for exploration and mining. European Journal of Mineralogy 24:863-878.

Masurel Q, Miller J, Hein KAA, Hanssen E, Thebaud N, Ulrich S, Kaisin J, Tessougue S (2016) The Yatela gold deposit in Mali, West Africa: The final product of a long-lived history of hydrothermal alteration and weathering. Journal of African Earth Sciences 113:73-87.

Masurel Q, Thebaud N, Miller J, Ulrich S, Hein K A.A, Cameron G, Beziat D, Bruguier O, Davis J (2017) Sadiola Hill: A World-Class Carbonate-Hosted Gold Deposit in Mali, West Africa. Economic Geology 112:23-47.

Kokaly RF, Clark RN, Swayze GA, Livo KE, Hoefen TM, Pearson NC, Wise RA, Benzel WM, Lowers HA, Driscoll RL, Klein AJ (2017) USGS Spectral Library Version 7 Data: U.S. Geological Survey data release, https://dx.doi.org/10.5066/F7RR1WDJ

Roache TJ, Walshe JL, Huntington JF, Quigley MA, Yang K, Bil BW, Blake KL, Hyvarinen T (2011) Epidote-clinozoisite as a hyperspectral tool in exploration for Archean gold. Australian Journal of Earth Sciences 58:813-822.

Van Ruitenbeek, FJA, Cudahy, T, Hale, M, van der Meer, FD (2005) Tracing fluid pathways in fossil hydrothermal systems with near-infrared spectroscopy. Geology 33(7):597–600.

van Ruitenbeek, FJA, Cudahy TJ, van der Meer FD, Hale M (2012) Characterization of the hydrothermal systems associated with Archean VMS-mineralization at Panorama, Western Australia, using hyperspectral, geochemical and geothermometric data. Ore Geology Reviews 45:33-46.

van Ruitenbeek, FJA, van der Werff HMA, Bakker WH, an der Meer FD, Hecker CH, Hein KAA (2017) Rapid classification of infra-red hyperspectral imagery of rocks with decision trees and wavelength images. http://www.itc.nl/library/papers_2017/pres/vanruitenbeek_rap_ppt.pdf

Wang R, Cudahy T, Laukamp C, Walshe JL, Bath A, Mei Y, Young C, Roache TJ, Jenkins A, Roberts M, Barker A, Laird J (2017) White Mica as a Hyperspectral Tool in Exploration for the Sunrise Dam and Kanowna Belle Gold Deposits, Western Australia. Economic Geology 112:1153-1176

Application of ASTER Data for Exploration of Porphyry Cu-Au Deposits in the Neoproterozoic Arabian–Nubian Shield: a Case Study from Egypt

Hamdy El Desouky
Geology Department, Faculty of Science, Menoufia University, Menoufia, Egypt
Egyptian Academy of Scientific Research & Technology, Cairo, Egypt

Abstract. Porphyry deposits are the world's most important source of Cu and Mo and are major sources of Au, Ag and Sn. The deposits are characterized by widespread and distinctive hydrothermal alteration zones, which provide a useful footprint for exploration. The Arabian-Nubian Shield (ANS), the Earth's largest tract of juvenile Neoproterozoic crust, has an apparent lack of porphyry Cu-Au deposits. In this study, detailed image processing techniques were performed in ASTER satellite imagery to identify the hydrothermal alterations associated with Cu-Mo-Au mineralization in the South Um Mongul Porphyry System (SUMPS), in the northern Eastern Desert of Egypt, to enhance exploration of porphyry systems in the ANS. The hydrothermal alterations detected by the ASTER image processing techniques have shown a good correspondence with the hydrothermal alteration zones reported in the field at SUMPS. Moreover, when the techniques are expanded to cover a larger area surrounding the SUMPS, new undiscovered hydrothermal alteration zones have been detected. This imply that the applied ASTER image processing techniques are robust enough for mapping porphyry hydrothermal alterations, especially in the arid to semi-arid regions of the ANS (e.g., Egypt).

1 Introduction

Porphyry deposits are the world's most important source of Cu and Mo and are major sources of Au, Ag and Sn. They account for about 50-60% of world Cu production and more than 95% of world Mo production (Sillitoe 2010). Porphyry deposits are large, low- to medium-grade deposits, which are spatially and genetically related to felsic−intermediate porphyritic intrusions. The deposits are characterized by widespread and distinctive hydrothermal alteration zones, which provide a useful footprint for exploration (Abrams et al. 1983; Sillitoe 2010). Recent reviews of the porphyry system characteristics are provided by Cooke et al. (2005), John et al. (2010), Sillitoe (2010) and Wilkinson (2013). Because Cu porphyry deposits generally form in the upper crust, at less than 5-10 km paleodepths, in tectonically unstable convergent plate margins and are prone to erosion, more than 90% of known deposits are Cenozoic or Mesozoic in age.

The ANS, which extends from Egypt in the west to Saudi Arabia and Oman in the east and from Jordan in the north to Eritrea and Ethiopia in the south, constitutes Earth's largest tract of juvenile Neoproterozoic crust (Fig 1). The ANS has an apparent lack of porphyry Cu-Au deposits (e.g., Ahmed and Gharib 2016; Khalifa et al. 2016; Bierlein et al. 2016a,b; Abd El-Rahman et al. 2018) compared with its abundant orogenic gold deposits, which have been mined in Egypt for over 7,000 years (Botros 2004, 2015; Klemm and Klemm 2013). This lack is related either to preservation problems during tectonics or to lack of relevant exploration programs in the huge terrains of the ANS.

The recent free data availability of the remote sensing multi-spectral Advanced Spaceborne Thermal Emission and Reflection Radiometer (ASTER; NASA 2001), offer geologists a potentially cost-effective alternative to expensive and time-consuming regional mineral exploration. Recent studies indicate that ASTER data can be used to map the hydrothermal alterations associated with porphyry ore deposits (e.g., Pour and Hashim 2011; Alimohammadi et al. 2015).

In this study, detailed image processing techniques were performed on ASTER satellite imagery to identify the hydrothermal alterations associated with Cu-Mo-Au mineralization in the SUMPS in the northern Eastern Desert of Egypt. The SUMPS was under exploitation for copper and gold during the Predynastic (ca. 3000 BC) and Arab (ca. 1350 AD) Periods (Klemm and Klemm 2013) and currently under development for reopening (Abd El-Rahman et al. 2018). The area has a well-defined surface geology, hydrothermal alteration and mineralization (Abd El-Rahman et al. 2017, 2018; Botros and Wetait 1997; Wetait and Botros 1997; Fig. 1). The results obtained from this test case study will enhance exploration of porphyry Cu-Au systems in the ANS.

2 Geology and Mineralization

The ANS is a north-south belt of folded, sheared, thrusted, and mostly moderately metamorphosed Neoproterozoic rocks of juvenile crust and represents an area of suturing between East and West Gondwana before the Paleozoic (Stern 1994). It formed through the accretion of numerous, mainly inter-oceanic, island arcs along ophiolite-lined suture zones and gneissic fault zones between 900 Ma and 550 Ma when the Mozambique ocean closed (Stern 1994). The basement rocks of the Eastern Desert of Egypt constitute the extreme northwestern part of the ANS.

The SUMPS is located in the northern segment of the Eastern Desert (Fig. 1a), which is characterized by lithologies with continental affinities, namely Dokhan

Volcanics and Hammamat Sediments (Hassan and Hashad 1990), and by abundant granitic intrusions (Fig. 1b). It lacks lithologies with oceanic affinities, such as ophiolitic assemblages, which are common in the central segment of the Eastern Desert (Abd El-Rahman et al. 2017, 2018). The SUMPS is occupied by Tonian porphyritic dacite (773 ± 6.9 Ma) with continental arc tectonic setting intruded by Ediacaran post-collisional hornblende gabbro (603 ± 3.5 Ma) and monzogranite (558 ± 4.6 Ma; Abd El-Rahman et al. 2017; Fig. 1c).

According to Abd El-Rahman et al. (2018), there are two porphyry mineralization systems in the SUMPS. The older is a Cu-Mo porphyry-style, which is related temporally to the Tonain dacite (773 ± 6.9 Ma). This system is characterized by the presence of quartz-chalcopyrite-molybdenite veinlets associated with biotite-dominated potassic alteration. The younger system, which overprints the older one, is related to the Ediacaran post-collisional monzogranite (558 ± 4.6 Ma) and is similar in many aspects to the iron oxide-rich Cu-Au porphyry-style. This younger system evolved from quartz-magnetite veins with potassic selvages to quartz-specularite and barite-specularite veins associated with more pervasive sericite-chlorite alteration (Abd El-Rahman et al. 2018).

3 ASTER Data

A cloud-free scene of ASTER Level 2 Surface Reflectance VNIR and SWIR V003 (AST_07) covering the study area was obtained from NASA (2001). The scene was acquired daytime in 29 April 2001 and pre-georeferenced to UTM zone 36 north projection using the WGS-84 datum. Radiometric, geometric and atmospheric corrections were applied on the image data. The SWIR data were further corrected for cross-talk and parallax errors due to the spatial locations of SWIR bands. The ASTER Level 2 Surface Reflectance image is composed of 9 spectral bands with different spatial resolutions (3 VNIR at 15m and 6 SWIR at 30m; Table 1; NASA 2001). Spectral resampling has been used to downscale the spatial resolution of the 6 SWIR ASTER bands to 15m resolution, then, the data has been resized to the coordinates of the SUMPS and the surrounding basement rocks (e.g., Fig. 3). The ASTER data was processed and analyzed by the ENVI (Environment for Visualizing Images) software package.

4 ASTER Image Processing

Several robust and reliable image-processing techniques, including, principal component analysis (PCA), minimum noise fraction (MNF), band ratio and band math were applied based on spectral characteristics of alteration key minerals for a systematic selective extraction of hydrothermal alteration zones in the SUMPS area and the surrounding areas. The processed images were displayed in RGB color channels to generate false color composites in order to highlight the hydrothermal alteration zones. The results of ASTER image processing were compared with the well-known hydrothermal alteration of SUMPS for validation (Fig. 1c; Abd El-Rahman et al. 2018; Botros and Wetait 1997).

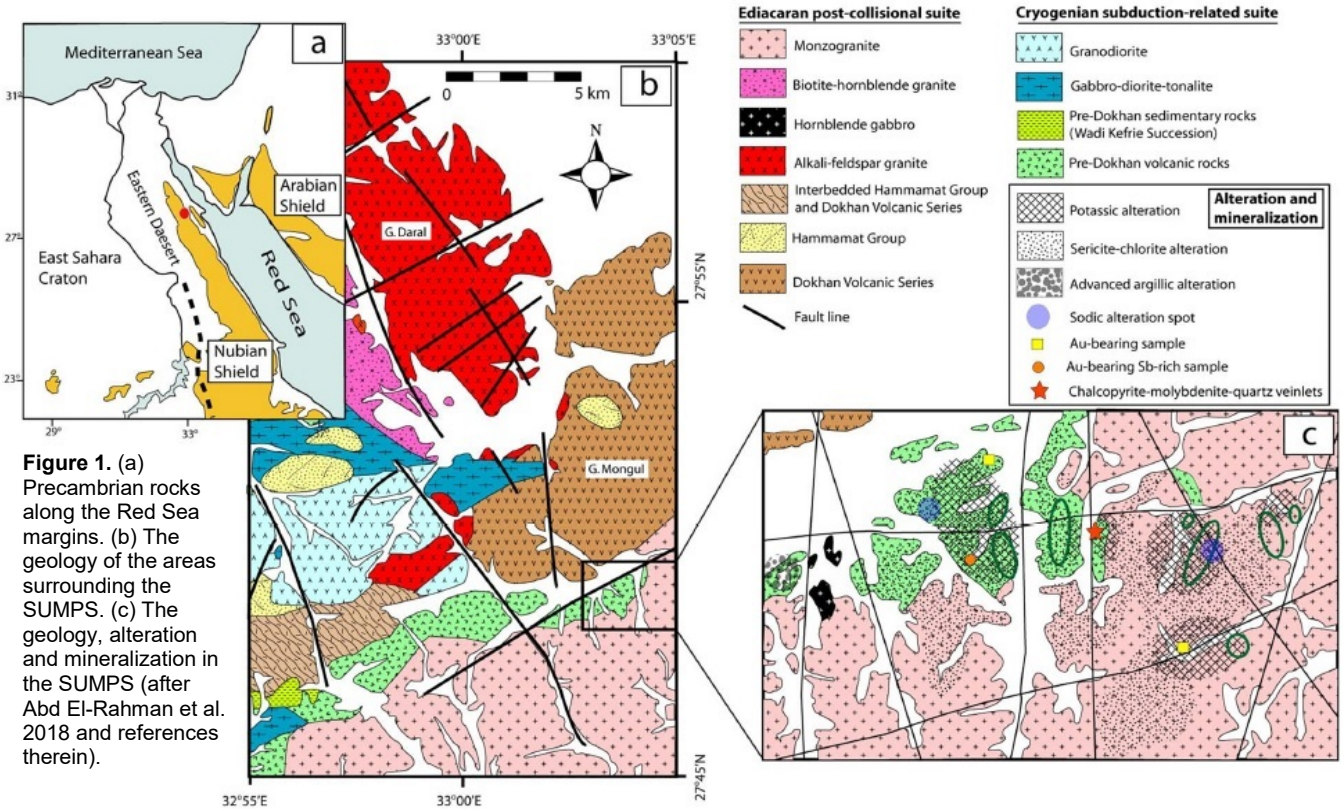

Figure 1. (a) Precambrian rocks along the Red Sea margins. (b) The geology of the areas surrounding the SUMPS. (c) The geology, alteration and mineralization in the SUMPS (after Abd El-Rahman et al. 2018 and references therein).

Table 1: ASTER VNIR and SWIR sensor characteristics.

Bands	Wavelength (μm)	Description	Res. (m)
VNIR_Band1	0.520 to 0.600	Visible (G/Y)	15
VNIR_Band2	0.630 to 0.690	Visible (R)	15
VNIR_Band3N	0.760 to 0.860	Near infrared	15
SWIR_Band4	1.600 to 1.700	Short-wave infrared	30
SWIR_Band5	2.145 to 2.185		30
SWIR_Band6	2.185 to 2.225		30
SWIR_Band7	2.235 to 2.285		30
SWIR_Band8	2.295 to 2.365		30
SWIR_Band9	2.360 to 2.430		30

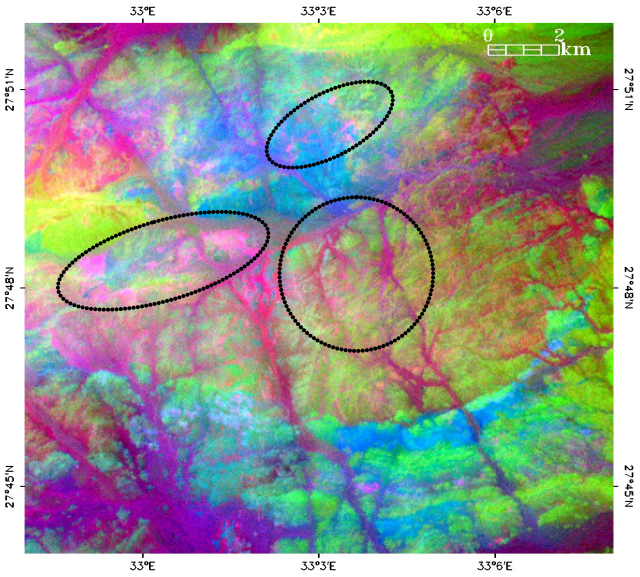

Figure 2. MNF composite image of transformation bands 312 in RGB. Areas with hydrothermal alteration are outlined by a circle at SUMPS and by ovals in the surrounding areas.

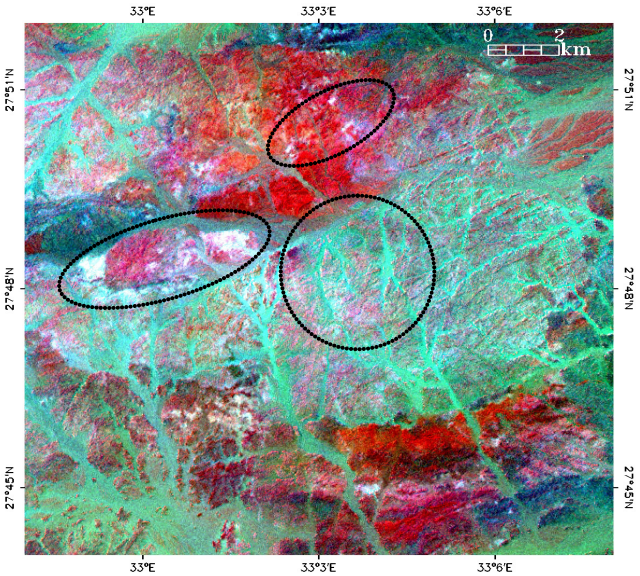

Figure 3. Band ratio composite image of ASTER bands 4/2, 4/5, 5/6 in RGB. Areas with hydrothermal alteration are outlined by a circle at SUMPS and by ovals in the surrounding areas.

PCA is a multivariate statistical technique that selects uncorrelated linear combinations (eigenvector loadings) of variables in such a way that each component successively extracted linear combination and has a smaller variance (Chang et al. 2006). A standard PCA transformation was applied to the VNIR and SWIR ASTER data.

The MNF transformation is used to determine the inherent dimensionality of image data, segregate noise in the data, and reduce the computational requirements for subsequent processing (Green et al. 1988). A standard MNF transformation was applied to the VNIR and SWIR ASTER data (Fig. 2).

Band ratio is a technique where the digital numbers (DN) of one band are divided by the DN values of another band. This technique is very useful for highlighting certain features or materials that cannot be seen in the raw bands (e.g., Inzana et al. 2003). A large number of band ratios was performed in the ASTER data, the best results include: 4/2, 4/5, 5/6 in RGB (Fig. 3); 4/5, 4/6, 4/7 in RGB (Fig. 4) and 5/6, 7/6, 7/5 in RGB.

Band math is a technique, which allow inserting the DN values of bands in mathematical formulas, e.g., to calculate the minerallogic indices of Ninomiya (2003). The performed indices include, the OH bearing altered minerals index (OHI = 7/6*4/6), the kaolinite index (KLI = 4/5*8/6), the alunite index (ALI = 7/5*7/8) and the calcite index (CLI = 6/8*9/8).

The ASTER image-processing techniques, which have shown good correspondence with field data at SUMPS were re-applied to a larger area of the basement rocks to test the technique in exploring areas with similar hydrothermal alteration to SUMPS (Fig. 5).

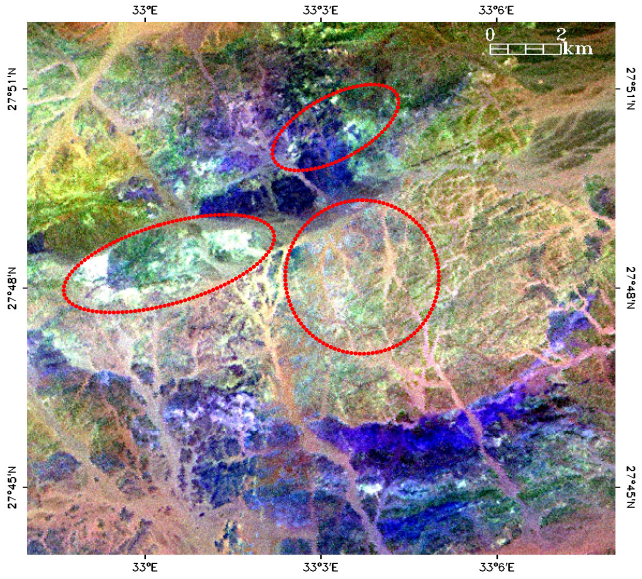

Figure 4. Band ratio composite image of ASTER bands 4/5, 4/6, 4/7 in RGB. Areas with hydrothermal alteration are outlined by a circle at SUMPS and by ovals in the surrounding areas.

5 Discussions

The performed ASTER image processing techniques allowed detecting a hydrothermal alteration zone in the area of SUMPS (Figs. 2-4). In this zone, the hydrothermal alteration minerals are intercalated with unaltered rocks in accordance with field observations and mapping (Abd El-Rahman et al. 2018; Botros and Wetait 1997; Wetait and Botros 1997; Fig. 1c). In addition to this zone, at least two other hydrothermal alteration zones were detected at

the north and northwest of the SUMPS (Figs. 2-4). These zones could be related to the same porphyry system or to an undiscovered epithermal system. Moreover, when the technique is expanded to cover a larger area surrounding the SUMPS (Fig. 5), more hydrothermal alteration zones with apparent similar characteristics to the zones of SUMPS have been detected. These zones could represent undiscovered porphyry systems. This imply that the applied ASTER image processing techniques are robust enough for mapping regional hydrothermal alterations, which footprint porphyry copper systems, especially in arid to semi-arid regions of the ANS (e.g., Egypt).

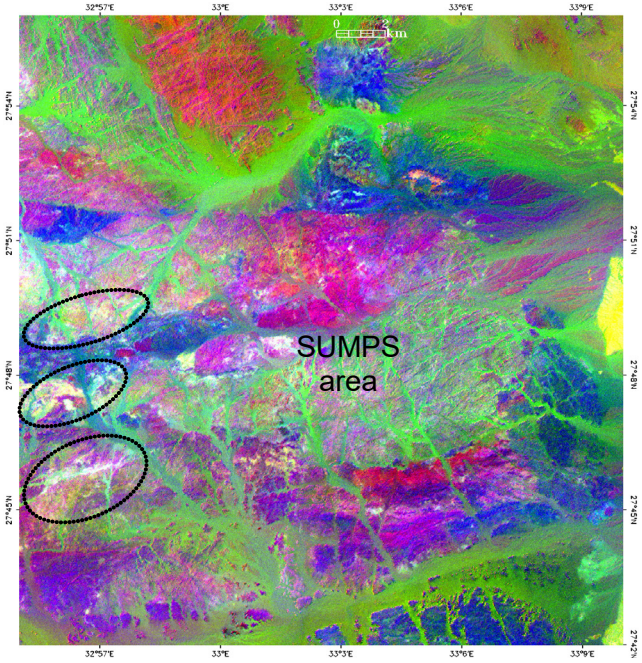

Figure 5. Band ratio composite image of ASTER bands 4/2, 4/5, 5/6 in RGB, applied to the area surrounding the SUMPS. Hydrothermal alterations similar to SUMPS are outlined by ovals.

Acknowledgements

The financial support of the Egyptian Academy of Scientific Research & Technology and the Menoufia University is highly acknowledged.

References

Abd El-Rahman Y, Seifert T, Gutzmer J, Said A, Hofmann M, Gärtner A, Linnemann U (2017) The South Um Mongul Cu-Mo-Au prospect in the Eastern Desert of Egypt: from a mid-Cryogenian continental arc to Ediacaran post-collisional appinite-high Ba-Sr monzogranite. Ore Geol Rev 80: 250−266.

Abd El-Rahman Y, Seifert T, Said A (2018) The South Um Mongul Cu-Mo-Au prospect in the northern Eastern Desert of Egypt: Tonian porphyry-style mineralization with an Ediacaran hydrothermal iron oxide overprint. Ore Geol Rev 99: 217−234.

Abrams MJ, Brown D, Lepley L, Sadowski R (1983) Remote sensing for porphyry copper deposits in southern Arizona. Econ Geol 78: 591−604.

Ahmed, AH, Gharib ME (2016) Porphyry Cu mineralization in the eastern desert of Egypt: inference from geochemistry, alteration zones, and ore mineralogy. Arab J Geosci 9: 179.

Alimohammadi M, Alirezaei S, Kontak DJ (2015) Application of ASTER data for exploration of porphyry copper deposits: A case study of Daraloo–Sarmeshk area, southern part of the Kerman copper belt, Iran. Ore Geol Rev 70: 290−304.

Bierlein FP, McKeag S, Murphy FC, Bargmann C, Bullen W, Al-Athbah H, Reynolds N, Brauhart C, Meffre S, McKnight S (2016a) The Jebel Ohier deposit —a newly discovered porphyry copper-gold system in the Neoproterozoic Arabian Nubian Shield, Red Sea Hills, NE Sudan. Miner Deposita 51: 713−724.

Bierlein FP, Reynolds N, Arne D, Bargmann C, McKeag S, Bullen W, Al-Athbah H, McKnight S, Mass R (2016b) Petrogenesis of a Neoproterozoic magmatic arc hosting porphyry Cu-Au mineralization at Jebel Ohier in the Gebeit Terrane, NE Sudan, Ore Geol Rev 79: 133−154.

Botros NS (2004) A new classification of the gold deposits of Egypt. Ore Geol Rev 25: 1−37.

Botros NS (2015) Gold in Egypt: does the future get worse or better? Ore Geol Rev 67: 189−207.

Botros NS, Wetait MA (1997) A possible porphyry copper mineralization in South Um Monqul, Eastern Desert, Egypt. Egypt J Geol 41: 175−196.

Chang Q, Jing L, Panahi A (2006) Principal component analysis with optimum order sample correlation coefficient for image enhancement. Int J Remote Sens 27 (16): 3387−3401.

Cooke DR, Hollings P, Walshe JL (2005) Giant porphyry deposits: Characteristics, distribution, and tectonic controls: Econ Geol 100: 801−818.

Green AA, Berman M, Switzer P, Craig MD (1988) A transformation for ordering multispectral data in terms of image quality with implications for noise removal. IEEE Trans Geosci Remote Sens 26 (1): 65−74.

Hassan MA, Hashad AH (1990) Precambrian of Egypt. In: Said R (ed) The geology of Egypt. A. A. Balkema, Rotterdam, Brookfield, pp 201−245.

Inzana J, Kusky T, Higgs G, Tucker R (2003) Supervised classifications of Landsat TM band ratio images and Landsat TM band ratio image with radar for geological interpretations of central Madagascar. J Afr Earth Sci 37: 59–72.

John DA, Ayuso RA, Barton MD, Blakely RJ, Bodnar RJ, Dilles JH, Gray F, Graybeal FT, Mars JC, McPhee DK, Seal RR, Taylor RD, Vikre PG (2010). Porphyry Copper Deposit Model. U.S. Geological Survey Scientific Investigations Report 2010–5070–B, 169 pp.

Khalifa IH, Hegazi AM, Faisal, M (2016) Geological setting for porphyry copper deposits in calc-alkaline rocks: wadi Rofaiyed area, Sinai, Egypt. Arab J Geosci 9: 336.

Klemm R, Klemm D (2013) Gold and Gold Mining in Ancient Egypt and Nubia. Springer-Verlag, Berlin Heidelberg, 649 pp.

NASA / METI / AIST / Japan Space Systems and U.S. / Japan ASTER Science Team (2001). ASTER Level 2 Surface Reflectance VNIR and SWIR V003 (AST_07), Crosstalk Corrected SWIR. NASA EOSDIS Land Processes DAAC, http://dx.doi.org/10.5067/ASTER/AST_07.003.

Ninomiya Y (2003) A stabilized vegetation index and several mineralogic indices defined for ASTER VNIR and SWIR data. Proceedings of the IEEE International Geoscience and Remote Sensing Symposium (IGARSS 2003), Toulouse, France, 21–25 July 2003: vol 3, pp 1552−1554.

Pour AB, Hashim M (2011) Identification of hydrothermal alteration minerals for exploring of porphyry copper deposit using ASTER data, SE Iran. J Asian Earth Sci 42: 1309−1323.

Sillitoe RH (2010) Porphyry copper systems. Econ Geol 105: 3-41.

Stern RJ (1994) Neoproterozoic (900-550 Ma) arc assembly and continental collision in the East African orogen: implications for the consolidation of Gondwanaland. Annu Rev Earth Planet Sci 22: 319−351.

Wetait MA, Botros NS (1997) Barite mineralization in the south Um Monqul area, northern Eastern Desert, Egypt. J African Earth Sci 25: 485−489.

Wilkinson, JJ (2013) Triggers for the formation of porphyry ore deposits in magmatic arcs. Nat Geosci 6: 917−925.

Structural-geochemical vectors for cost-effective targeting of unconformity-type uranium mineralization: the Maverick uranium deposit case study

Ranee E. Joshi, Irvine R. Annesley[1], Gautier Laurent
Université de Lorraine

Christine L. McKechnie
Skyharbour Resources

Zoltan Hajnal
[1]University of Saskatchewan

Abstract. Bridging the gap between the increasing exploration cost, decreasing U_3O_8 spot price, and the number of new uranium discoveries, this paper presents new vectoring tools developed from an improved understanding of the Maverick uranium deposit (MUD), Athabasca Basin. These vectors include critical geochemical anomalies, structurally controlled fluid pathways, and/or structural-geochemical traps. Geochemical studies of the MUD, show a distinct zoning of alteration clay minerals around uranium mineralization. The fault damage zones can be correlated with major elements and trace elements, including Be, Ni, Zn, Rb, Nb, Ba, Ce, Sm, Eu and Tm. Gd and Tb are good vectors both in the basement and basin lithologies. Base metals are good indicators for proximity to uranium deposits, but their signatures are not evident above the sedimentary package. Sb, V, and Cd can be used to vector toward the uranium mineralization from the surface. Incorporating vectoring studies within an exploration company's business model provides multiple advantages. In the case of the MUD, an estimated exploration cost of ~3 million US$ could have been saved by reducing costly drilling programs in the early stages of exploration and focusing on structural mapping and near-surface geochemical sampling after the initial ~40-50 exploratory/discovery holes.

1 Introduction

Uranium oxide is a radioactive, silvery-white metal (element 92 in the periodic table) that has been used as a yellow-orange pigment for coloring glass, military purposes, and for electrical power generation. In 2003, a renewed interest due to its neutral impact on greenhouse gas emissions (Lehmann 2008) caused a ten-fold price hike; reaching a maximum price in June 2007 of US$135 per pound. However, the Fukushima Daiishi accident in Japan in 2011 slowed uranium activities with spot prices approaching near historic lows (Nuclear Energy Agency and International Atomic Energy Agency 2016). At present, the U_3O_8 price is at US$28/lb, after bottoming out US$18/lb in 2016.

There are many types of uranium deposits in the world that are subdivided based on their geological setting. Unconformity-type uranium deposits, which make up a third of uranium resources, have grades 3-100 times higher than any other types of deposit (Jefferson et al. 2007). The Athabasca Basin is the main host for unconformity-type deposits and has an estimated resource more than 373,000 t U (Thomas et al. 2000). Most of the known mineralization zones are located on the eastern side of the Athabasca Basin at, above, and/or below the unconformity. The uranium grades and tonnages of the Cigar Lake (15%, 131,000 tonnes) and McArthur River (22%, 192,000 tonnes) deposits in the Athabasca are very high, giving the whole Athabasca Basin an average grade of 1.97% (Jefferson et al. 2007). Given the high uranium grade and tonnage as well as the increase in uranium demand, exploration in the Athabasca has been very active. However, many of the recent discoveries have much lower grades and tonnages, i.e. Millennium deposit (4.53%, 18,000 tonnes). Exceptions to this would be the Phoenix deposit; one of the highest grade unmined deposits, and Arrow, the largest unmined deposit.

As newly discovered uranium deposits have significantly lower grades and the U3O8 market price is much lower, the price for exploration is consistently increasing. The cost of drilling alone ranges from 100 $/m to 350 $/m. This situation calls for improvements in the exploration process, wherein the available geological information is maximized, and the costs are reduced. This paper presents geochemical and structural signatures related to potentially mineralized uranium unconformity-type zones.

2 Geologic setting

The Maverick Uranium Deposit (MUD) occurs within the eastern Athabasca Basin (Saskatchewan, Canada), a Paleoproterozoic to Mesoproterozoic sedimentary basin in northern Saskatchewan and northeast Alberta (Jefferson et al. 2007). The Athabasca Basin is estimated to have a present-day maximal depth of around 1500 m (Györfi et al. 2007; Rainbird et al. 2007; Ramaekers et al. 2007). The basin was deposited between 1.76 Ga and 1.5 Ga (Ramaekers et al. 2007) above a regional angular unconformity separating unmetamorphosed flat-lying

nearly undisturbed sediments from the highly deformed and metamorphosed basement of the southwestern Churchill Province.

MUD's basement consists of deformed and metamorphosed Archean/Paleoproterozoic rocks of the Hearne subprovince of the western Churchill Province. The Hearne Province is separated from the Rae Province by the Snowbird Tectonic Zone (STZ), a continental scale Paleoproterozoic suture zone; the STZ is located close to the center of the Athabasca Basin (Hoffman 1988). The Hearne Province underwent high-grade deformation and metamorphism during the continent–continent collision of the Trans-Hudson Orogen (1.8 Ga) (Bickford et al. 1990; Card et al. 2007; Lewry and Sibbald 1980; among others). Structural studies of the eastern Athabasca region highlight four lithostructural domains from west to east (Annesley et al., 2005): Mudjatik Domain (MD), Wollaston-Mudjatik Transition Zone (WMTZ), Western Wollaston domain (WWD) and Eastern Wollaston Domain (EWD). The MUD straddles the transition between the Western Wollaston Domain (WWD) and Eastern Wollaston Domain (EWD) of the Athabasca Basin (Fig. 1), forming part of the former JNR Resources (now Skyharbour Resources) Moore Lakes Project.

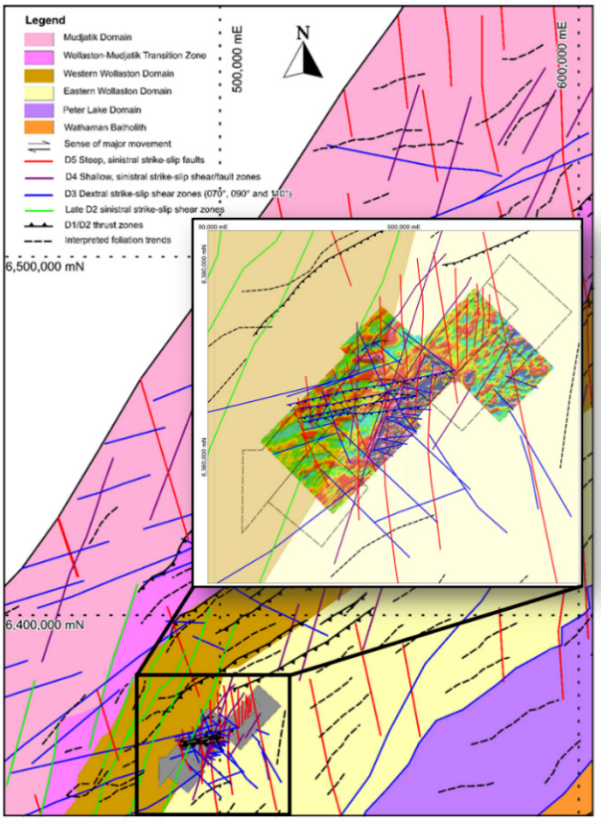

Figure 1. Lithotectonic domains of the Archaen-Proterozoic basement of southeastern Athabasca Basin (Modified from Annesley et. al, 2005; JNR Resources Inc. Mapinfo files) and inset showing closer look of the Moore Lakes Project overlain on magnetics vertical derivative data.

MUD is unconformably overlain by Athabasca sandstone with a thickness about 275 meters; the sandstone on the project generally thickens from the southeast to northwest. It lies above a well-defined east-west striking (80 degrees) paleotopographic high coinciding with the subvertical to inclined, dextral D3 strike-slip Maverick structure (Figs. 1 and 2). The Maverick Structure is an inferred to be a reactivated D1-D2 thrust fault. This early thrust is characterized by a graphitic unit between two basement rocks: Archean granite in the footwall and pelitic gneiss in the hanging wall. The Maverick mineralization occurs within the dipping graphitic unit with little or no offset (i.e. strike-slip system) and the majority of mineralization occurs at or above the unconformity, with limited basement-hosted mineralization. Potential for basement-hosted mineralization is unknown, although recently Skyharbour Resources has found some.

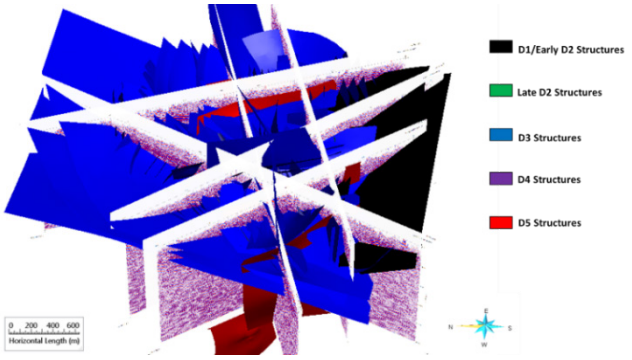

Figure 2. Maverick structural model showing different deformation stage structures.

3 Data available

The geochemical analysis is based mainly on JNR Resources Inc.'s geochemical and assay database, comprising historic data and unpublished assessment file data collected between 1997 and 2007. It is composed of 11956 measurements in 285 holes at and around the Maverick uranium deposit; including 252 mineralized drill holes. This unpublished data for the basin and the basement were made available from assessment file downloads by the 2nd author for the 1st author's Master's thesis project.

The ioGAS software was used for the geochemical modelling. Intensity of hydrothermal alteration zones and the degree of magmatic differentiation in the basement intrusive rocks (i.e. potential source rocks) were assessed through geochemical modeling. In addition, erratic U anomalies were correlated with minor and trace elements to vector towards mineralization.

4 Unconformity-type uranium vectors

4.1 Alteration mineral assemblages

The clay alteration observed in MUD is defined by distinct alteration haloes continuing to the top of the Manitou Falls graphitic pelitic gneisses are weakly to intensely altered, including within localized intervals where graphite is partially to completely destroyed and carbonaceous matter is deposited hydrothermally. Within the basin, the Maverick structure is surrounded by a damage zone which comprises intensely altered, desilicified, bleached Manitou Falls sandstone. This zone

is strongly altered to kaolinite and dravite, and extends upwards to ~140 meters above the unconformity. In the basement, the variably altered (to clay minerals and secondary chlorite) crystalline rocks include a number of sheared, brecciated, and fault-gouged intervals. Around this highly faulted zone is a broad illite halo extending about 120 meters from the fault core. The outer shell of the alteration (i.e. the least structurally disturbed zones) changes abruptly to dickite-dominated.sandstone (Fig. 3). It extends laterally throughout the Maverick structure and downward to the unconformity at about 275 meters. This suggests that the alteration feature is controlled by the orientation and dip of the Maverick structure, coinciding in part with the graphitic pelitic gneiss. The

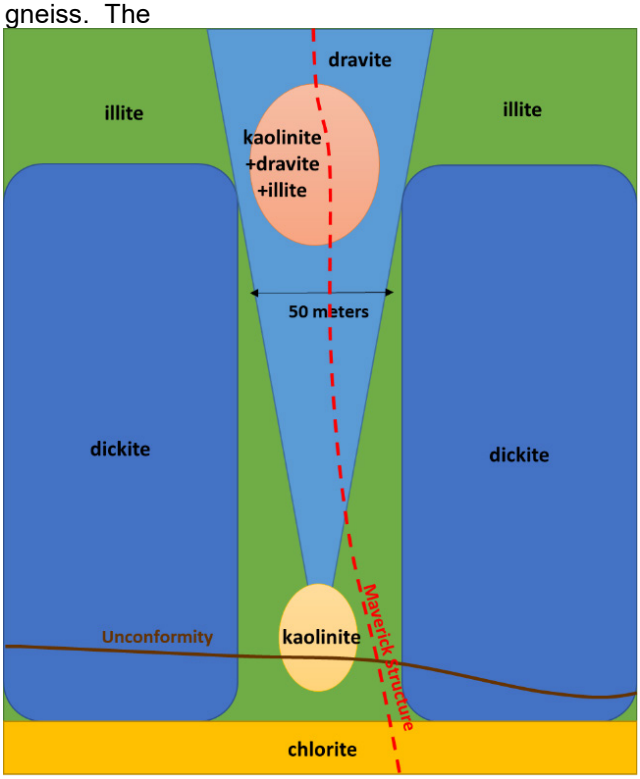

Figure 3. Simplified schematic diagram showing the different alteration haloes in the Maverick Uranium Deposit.

4.2 Geochemical signatures

To understand the geochemical anomalies related to the uranium mineralization, the correlation between U% and major and trace elements was computed to help recognize the geochemical signature of the MUD. The data from MUD confirms expected correlation between uranium and base metals such as Pb, Co, Ni, Zn and Cu. Mineralized samples (>0.005% U) correlate with Pb, Co, Hg, Pr, V, Sm, Sc, Sn, Dy, Bi, Yb and Eu. MFa, the main host of mineralization varies well with Hg, Pr, Pb, Co, Ni, Zn, V, Sm, Dy, Bi, Th, Tb, Gd, Er. The uranium in clay varies strongly with Tb. Uranium in mineralized graphitic pelitic gneisses also varies with Sb and As.

The mineralized and fault-damaged zones can be correlated with Na_2O, MgO, K_2O, CaO, MnO, P_2O_5, Fe_2O_3, Be, Ni, Zn, Rb, Nb, Ba, Ce, Sm, Eu, Gd and Tm anomalies. The electomagnetic (EM) conductors and their associated lithologies are locally structurally disrupted, clay-altered, and anomalous in Cu, Pb, Ni, Zn and V (i.e. pathfinder elements).

Initial Principal Component Analysis (PCA) studies revealed possible pathfinder elements that are not lithologically restricted. The ranked attributes obtained are Li, Dy, Gd, Tb, Nd, Co, Pb, Cu, Zn, and Ni. These results further support uranium's positive correlation with base metals and provide trace elements to focus on. The results show that uranium content can be best correlated with Gd content (Fig. 4). The correlation between U and Gd is 0.70. It is interesting to note that this correlation is observed both in basement and basin lithologies. Tb also showed good correlation with U (0.56). However, it could be noticed that this relationship works better for basement rocks. Other correlations can also be used (e.g. U vs Pb).

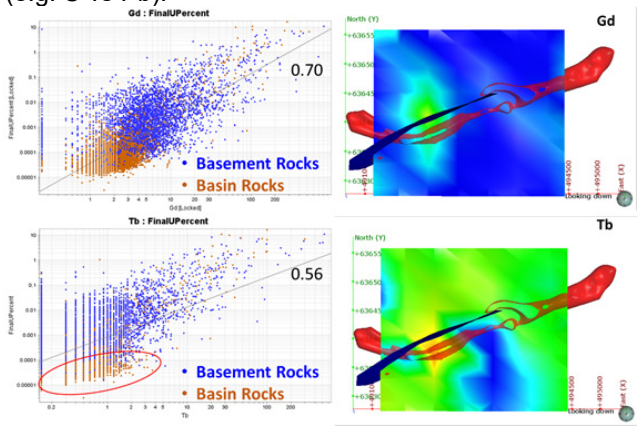

Figure 4. U-Gd (top) and U-Tb (bottom) molar ratio plots show that U values are well correlated with Gd and Tb both for basement and basin rocks. The correlation for Tb is lower due to its relationship with unmineralized basin rocks (red ellipse). The corresponding spatial distribution of U and Tb content in relation to the ore zone and unconformity surface.

5 Economic impact

To assess the economic benefits of using geochemical and structural vectors as a major step in uranium unconformity-type exploration, a comparative cost analysis on the Moore Lakes Project has been carried out. The cost analysis utilizes the following cost estimates from Lahusen et al. (2016) and McKechnie (pers. Comm.):

Drilling speed=	4 meters/hour
Drilling costs=	$150/meter
Fuel cost=	$1/liter
Labor cost=	$50 /hour
Boron analysis cost=	$30/sample
Elemental analysis cost=	$150/sample

In the conventional exploration cost analysis, it was assumed that no separate near-surface geochemistry was conducted. Instead 320 drillholes (35 exploratory drill holes for entire Moore + 285 delineation drillholes in Maverick; 100 samples per hole) in the Moore Lakes project were drilled and analyzed for U, B SiO_2, C, S and other elements with an Inductively Coupled Plasma Mass Spectrometer (ICP-MS). On the other hand, the cost analysis for the exploration using geochemical vectoring,

uses near-surface drilling (i.e. <400 meters; U/C at ~275 meters) on the entire Moore Lakes project (Fig. 5). Using the current distribution of drillholes, it is estimated that about 50 drillholes would have covered the explored part of Moore Lakes project. From the distributed 50 holes, the Maverick zone would have been found to be anomalous and indicative for a potential deposit. Continuing with definitive drilling, the cost analysis uses 285 holes which are enclosed within the MUD. The results of this cost analysis show that the exploration costs of discovering/delineating the MUD could have been $26.4M instead of $29.5M USD; a potential cost savings of $3M USD. This supports the use and effectiveness of the geochemical vectoring tools.

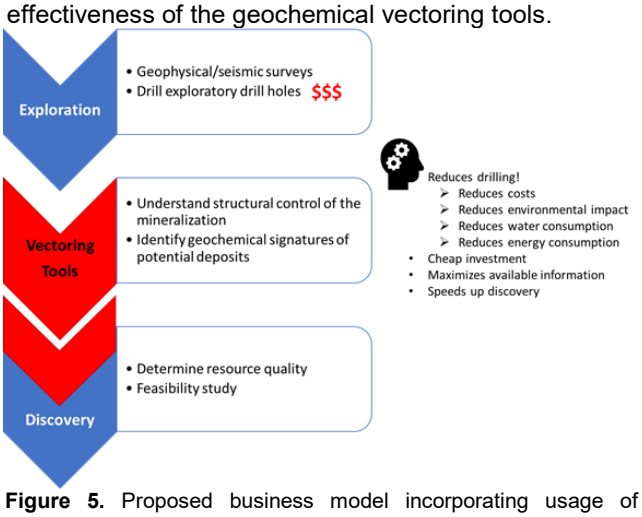

Figure 5. Proposed business model incorporating usage of vectoring tools in early exploration of uranium unconformity-related deposits.

6 Conclusions and recommendations

This study encourages maximizing publicly-available data to build a geologic and geochemical model that may provide vectoring tools for unconformity-type uranium deposits. MUD provides an example of doing this and tests existing geochemical vectors. The results strongly suggest that incorporating these vectoring tools in an exploration company's program may be one of several solutions the industry may take in bridging the gap between increasing exploration process and lower metal grades. It is important to note that although much care has been taken into verifying the data sets used to define the vectoring tools, it is yet to be tested in other nearby discovered and undiscovered uranium deposits of the eastern Athabasca Basin.

Acknowledgements

This work has been made possible thanks to the EMerald program, a 2-year Erasmus Mundus Master in Georesources Engineering. We would like to thank the host university, the École Nationale Supérieure de Géologie (ENSG), Université de Lorraine, CNRS, and GeoRessources (Nancy, France). We would also like to acknowledge the RING team lab for providing access to the SKUA-GOCAD and ioGAS licenses.

References

Annesley IR, Madore C, Portella P (2005) Geology and thermotectonic evolution of the western margin of the Trans-Hudson Orogen: evidence from the eastern sub-Athabasca basement, Saskatchewan Canadian Journal of Earth Sciences 42:573-597 doi:10.1139/E05-034

Bickford ME, Collerson KD, Lewry JF, Vanschmus WR, Chiarenzelli JR (1990) Proterozoic Collisional Tectonism in the Trans-Hudson Orogen, Saskatchewan Geology 18:14-18 doi:Doi 10.1130/0091-7613(1990)018<0014:Pctitt>2.3.Co;2

Card CD, Pană D, Portella P, Thomas DJ, Annesley IR (2007) Basement rocks to the Athabasca basin, Saskatchewan and Alberta Bulletin of the Geological Survey of Canada:69-87

Györfi I, Hajnal Z, White DJ, Takacs E, Reilkoff B, Annesley IR, Powell B, Koch R (2007) High-resolution seismic survey from the mcarthur river region: Contributions to mapping of the complex P2 uranium ore zone, athabasca basin, saskatchewan Bulletin of the Geological Survey of Canada:397-412

Hoffman PF (1988) United Plates of America, the Birth of a Craton - Early Proterozoic Assembly and Growth of Laurentia Annual Review of Earth and Planetary Sciences 16:543-603 doi:DOI 10.1146/annurev.ea.16.050188.002551

Jefferson CW, Thomas DJ, Gandhi S, Ramaekers P, Delaney G, Brisbin D, Cutts C, Quirt D, Portella P, Olson RA (2007) Unconformity-associated uranium deposits of the Athabasca basin, Saskatchewan and Alberta Bulletin of the Geological Survey of Canada:23-67

Lahusen L, Stewart P, Kyser K, Dunn C, Stacey P (2016). The utility of surface geochemistry - The model. Technical report, Uravan Minerals, Athabasca Basin, Saskatchewan (Canada).

Lehmann, B. (2008). Uranium ore deposits. Reviews in Economic Geology, pages 16–26.

Lewry JF, Sibbald TII (1980) Thermotectonic Evolution of the Churchill Province in Northern Saskatchewan Tectonophysics 68:45-82 doi:Doi 10.1016/0040-1951(80)90008-6

Nuclear Energy Agency and International Atomic Energy Agency (2016). Uranium 2016: Resources, production and demand. Technical report, Nuclear Energy Agency/International Atomic Energy Agency.Lehmann B (2008) Uranium ore deposits Rev Econ Geol AMS Online 16:2008

Rainbird R, Stern R, Rayner N, Jefferson C (2007) Age, provenance, and regional correlation of the Athabasca Group, Saskatchewan and Alberta, constrained by igneous and detrital zircon geochronology Bulletin-Geological Survey of Canada 588:193

Ramaekers P, Jefferson CW, Yeo GM, Collier B, Long DGF, Drever G, McHardy S, Jiricka D, Cutts C, Wheatley K, Catuneanu O, Bernier S, Kupsch B, Post, RT (2007) Revised geological map and stratigraphy of the Athabasca Group, Saskatchewan and Alberta Bulletin-Geological Survey of Canada 588:155

Thomas DJ et al. (2000) Athabasca Basin (Canada) unconformity-type uranium deposits: exploration model, current mine developments and exploration directions Geology and Ore deposits:15-18

Geophysical imaging of iron-oxide apatite deposits in the eastern Adirondacks, northern New York

A.K. Shah[1], R.D. Taylor[1] and G.J. Walsh[2]
[1]U.S. Geological Survey, Denver, Colorado, U.S.A.; [2]U.S. Geological Survey, Montpelier, Vermont, U.S.A.

Abstract. We present results of airborne geophysical surveys, ground geophysical measurements, and laboratory analyses of rocks collected in the magnetite-apatite "Kiruna-type" deposits of the eastern Adirondack Mountains in northern New York. Airborne radiometric data mostly reflect the surface geology, but the most prominent anomalies are equivalent Th and U (eTh and eU) highs over large tailings piles, a residual of extensive mining activity in the 1800s and 1900s. These tailings piles contain rare earth element (REE)-bearing apatite, consistent with a correlation between REEs and Th in samples. Widespread K anomalies observed at iron-oxide-apatite deposits elsewhere and attributed to potassic alteration are not present, probably because of overprinting by later sodic alteration. The magnetic field is dominated by a broad high that corresponds mostly to magnetite-rich leucogranite host rock. High-pass filtering of magnetic flight line data reveals numerous anomalies associated with known magnetite deposits, although in some areas smaller leucogranite bodies are also highlighted. 3-D inversions for magnetic susceptibility show general shapes, orientation, and relative dimensions of the deposits that are consistent with published reports. Together these analyses show how geophysical surveys can be used for exploration, mapping the distribution of deposits, and as a remote sensing tool for REEs in tailings.

1 Introduction

The eastern Adirondacks in northeastern New York contain dozens of low-Ti, REE-bearing "Kiruna-type" iron-oxide-apatite (IOA) deposits that provide an excellent case study for geophysical exploration and 3-D imaging. These deposits were extensively mined for iron in the 1800s and 1900s, resulting in reasonable documentation of deposit locations and in some cases their subsurface extent (Kemp and Ruedemann 1910; Farrell 1996). Mining activities also resulted in numerous waste and tailings piles containing REE-bearing apatite, presenting a possible "recycled" resource (McKeown and Klemic 1956; Mariano and Mariano 2012; Taylor et al. 2018a). The apatite is of marked interest because it contains elevated heavy rare earth minerals (Valley et al. 2011; Mariano and Mariano 2012; Lupulescu et al 2017; Taylor et al. 2018a).

Exploration and imaging of IOA and IOCG (iron-oxide-copper gold) deposits has been attempted using magnetic, gravity, and radiometric data, with success depending on the geologic setting and deposit mineralization. In the absence of sedimentary cover, radiometric data (gamma spectrometry for K, U, and Th) may show elevated K associated with potassic alteration (Shives et al. 2000; Sandrin et al. 2007). Magnetic and gravity data are more variable: Deposits in southeastern Missouri, northwestern Canada, Kiruna, Sweden, and Candelaria, Chile show local magnetic and sometimes local gravity highs, while deposits in the Gawler craton of Australia, which hosts the world-class Olympic Dam deposit, show gravity highs and weaker or offset magnetic anomalies (Rutter and Esdale 1985; Smith 2002; Clark 2003; Sandrin and Elming 2006; Direen and Lyons 2007; Sandrin et al. 2007; Austin and Foss 2012; Hayward et al. 2013; McCafferty et al. 2016).

In December 2015 we collected airborne magnetic and radiometric data over a 70 km by 25 km area covering dozens of magnetite-apatite deposits. Over two subsequent field seasons we measured radiometric and magnetic susceptibility on outcrops and whole rock geochemistry on samples from deposits, host rock, waste, and tailing piles. Results of these data are used to examine how geophysical methods can assist exploration, to obtain 3-D views of individual deposits, and to examine the regional geologic context of the deposits.

2 Geologic Setting

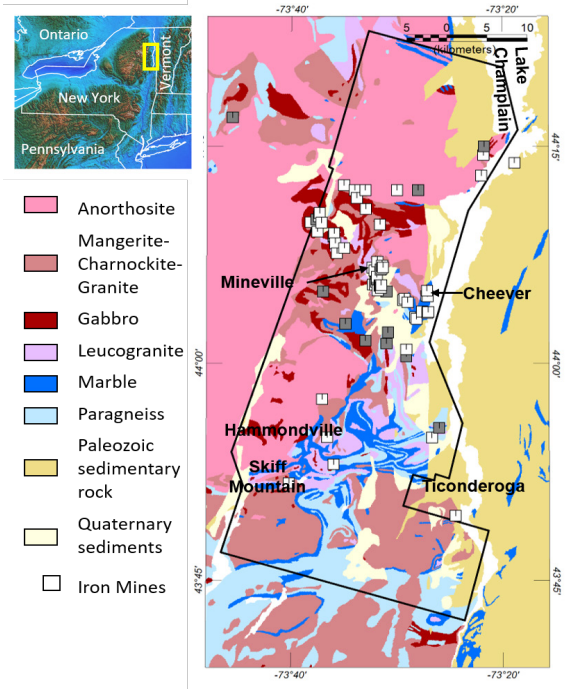

Figure 1. Simplified geologic map of the study area modified from Isachsen and Fisher (1970). Black polygon delineates the airborne geophysical survey bounds. Squares represent iron mines and prospects from the USGS Mineral Resources Database. Inset shows location in New York; yellow box shows the area of interest.

The magnetite-apatite deposits are located primarily on the northern and eastern edges of the dome-shaped Adirondack Mountains and hosted mostly in magnetite-rich leucogranite (with some exceptions). They are believed to have formed in the latter part of the Grenville orogeny during a phase of post-orogenic extensional collapse (Foose and McLelland 1995; Valley et al. 2011; Chiarenzelli et al. 2017). Other rocks in the region include a suite of anorthosite-mangerite-charnockite-granite (AMCG) and meta-sedimentary rocks, Paleozoic sedimentary cover to the east, and glacial cover in some areas (Fig. 1). We note an absence of copper and gold in economic quantities within the region indicating the deposits are more like the IOA deposits in Kiruna, Sweden (Valley et al. 2011).

Numerous deposits are present, often occurring in clusters. The largest and most productive of these are in the Mineville area with several lenticular, podlike, or tabular ore bodies whose long axes trend to the NNE deepen to the SSW (Kemp 1898). The presence of REE-bearing apatite within the deposits is highly variable over local scales, with deposits a few kilometers apart showing very different concentrations (McKeown and Klemic 1956; Valley et al. 2011; Lupulescu et al. 2017; Taylor et al. 2018a).

3 Methods

Airborne magnetic and radiometric surveys were flown in 2015 with a line spacing of 250-m and nominal terrain clearance of 125 m (Shah 2016). Ground truth measurements of magnetic susceptibility and radiometric properties of outcropping deposits, host rock, and tailings were collected. Samples of deposits, host rock, waste, and tailings were also analyzed for whole rock geochemistry (Taylor et al. 2018b).

Exploration approaches using magnetic data are challenging in the eastern Adirondacks because the magnetite-apatite deposits are mostly hosted by larger bodies of magnetite-rich leucogranite, which can mask deposit anomalies. We thus applied high-pass filtering approaches to the magnetic data with a goal of distinguishing shallow, very highly magnetic deposits from the leucogranite. This included a simple 1-D high-pass filter on flight-line data (Fraser et al. 1966) with a window size of 150 m to capture the shortest-wavelength anomalies. We note that this window is smaller than the flight line spacing and would likely create spurious results on gridded data. A steep regional magnetic inclination of 69° indicates that reduction to the pole has a very minor effect and anomalies should be closely aligned with their sources (assuming there is no large oblique remanent mag-netization component).

To image the subsurface shape, orientation, and relative extent of the deposits, we also developed 3-D inversions for magnetic susceptibility using the method of Phillips (2014). This approach inverts for susceptibility by minimizing an objective function describing the difference between the observed and calculated mag-netic fields. The inversions are intrinsically under-determined so a cubic depth-weighting constraint, which mimics the falloff of the magnetic field with distance to source, was applied. We note that the solution does not include effects of remanence or demagnetization, so results have limited quantitative accuracy without external constraints, especially if those effects are dominant. Nonetheless, they can still provide a qualitative 3-D view of the various deposits and their relative differences.

4 Results

4.1 Radiometric data

The most prominent feature of the aeroradiometric maps (Fig. 2) is a set of equivalent Th and U (eTh and eU) highs from Port Henry to Mineville. These each corres-pond to known tailings piles. In some areas these highs continue along roads, perhaps because some tailings are used for winter road gravel. Not all tailings piles in the region exhibit eTh-eU anomalies. Geochemical analyses of materials from a subset of these piles show that the eTh-eU highs occur where REE-bearing apatite concentrations are also high, reflecting a correlation between Th and REE (see also Taylor et al. 2018a). This correlation does not appear to apply to *in situ* deposits, however. While eTh is elevated in locales, it is usually over a broader scale than the deposits.

The radiometric data otherwise show broad, regional trends that mostly correspond with rock type, consistent with outcrop measurements. For example, anorthosite and gabbro have low K, eTh, and eU while carbonate

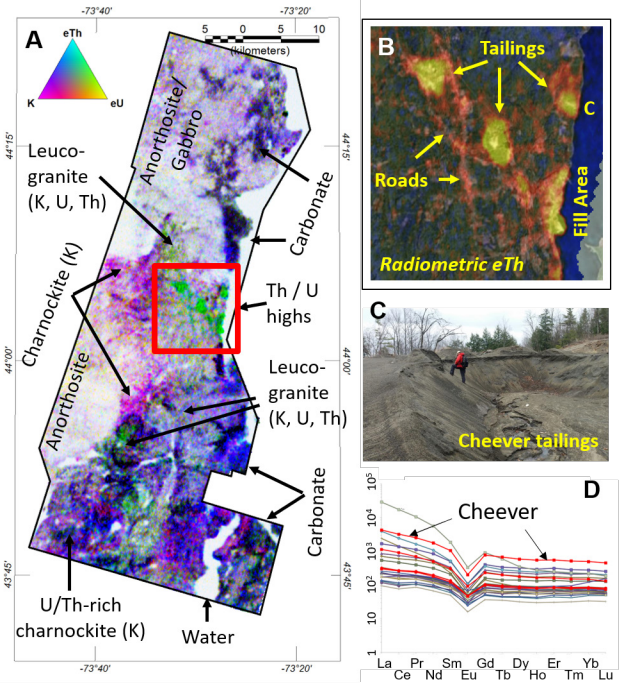

Figure 2. A. Ternary diagram of the radiometric data and corresponding rock types. Magenta=K, cyan=eTh, yellow=eU, green=eTh+eU. Red box shows location of (B). Equivalent Th over satellite image. "C" marks the Cheever mine. C. Photo of tailings at the Cheever mine. Photo by A. Shah, USGS. D. Chondrite-normalized concentrations of REEs for waste tailings. At Cheever, measured La, Ce, Nd, and Y were 1010, 1960, 807, and 867 ppm, respectively (see also Taylor et al. 2018b).

rocks are high in all three. Charnockite typically shows elevated K but eTh and eU are more variable. For the leucogranite, K, eTh, and eU are highly variable. We note that there are no regions with broad K anomalies as observed in other areas such as Kiruna and Canadian locales, attributed to potassic alteration (Shives et al. 2000; Sandrin et al. 2007). Sample analyses show that while potassic alteration has occurred, it has been mostly overprinted by sodic alteration (Valley et al. 2011).

4.2 Magnetic data

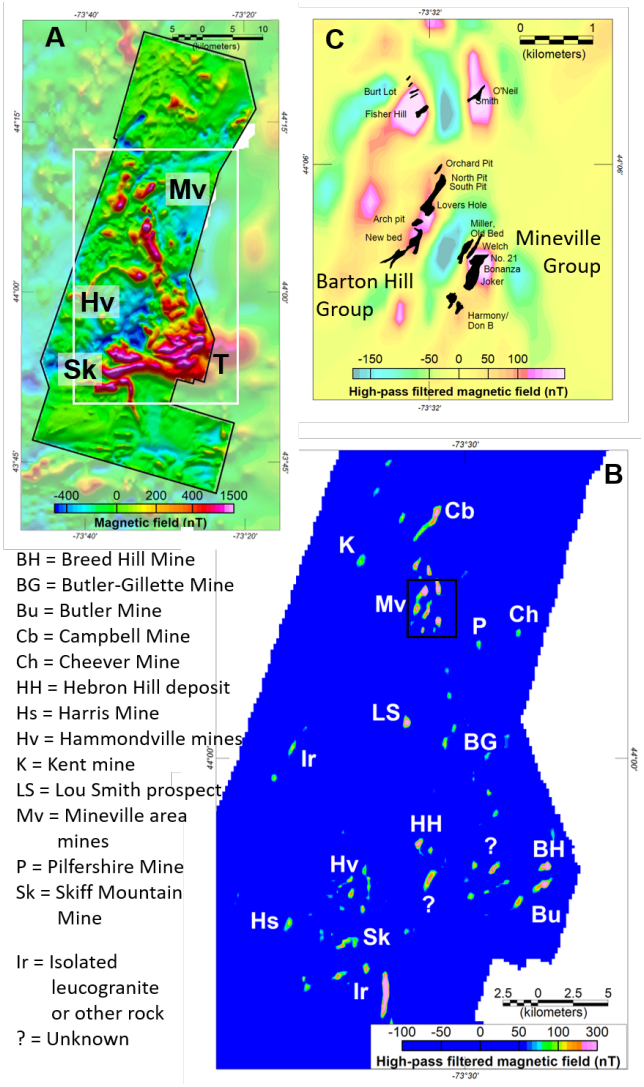

Figure 3. A) Magnetic field. Faded area shows previous regional survey data; black polygon delineates 2015 survey bounds. White box shows location of panel B. T = Ticonderoga, M = Mineville, Sk = Skiff Mountain, Hv = Hammondville. B) High-pass filtered magnetic field over central part of survey area and locations of some mines and prospects. Note color scale truncates lower values. Box shows location of panel C. C) Closeup of the Mineville area mines and high-pass filtered magnetic field. Black filled polygons represent estimated ore bodies by Kemp and Ruedemann (1910). Labels note associated pits and shafts that accessed the Barton Hill group and Mineville group ore bodies.

The magnetic anomaly (Fig. 3) is dominated by a broad, up to 1500 nT high near the town of Ticonderoga. The high has NNW- and W-trending branches extending towards Mineville and Skiff Mountain-Hammondville, respectively. The wider part of the high continues to the east, suggesting that the magnetic source continues beneath the Paleozoic cover. A comparison to surface geology shows that the high corresponds mostly to leucogranite (mapped partly beneath glacial cover near Mineville), consistent with leucogranite outcrop susceptibility measurements of 30-70x10^{-3} SI. There are more localized highs to the north which correspond to smaller bodies of leucogranite or gabbro (the magnetic susceptibility of gabbro averaged 1-8 x10^{-3} SI). The high also shows correspondences to major structures, with WNW- and W-trending lineaments near Hammondville and Skiff Mountain. The NNW branch towards Mineville is also notably linear.

The high-pass filtered magnetic field shows local highs ranging from about 100 to 350 nT (Fig. 3B). Most of these highs correspond to known magnetite-apatite deposits, many of which occur in clusters. Some highs are elongate, following structural trends. Some highs, however, represent narrow bodies of leucogranite against a background of less magnetic rock. In other areas the presence or absence of deposits isn't known. Near Mineville, where the subsurface extents of some deposits have been documented (Kemp 1898), the highs follow the broad shape of buried ore bodies, noting that the bodies are narrower than the survey flight line spacing, and some might not have been fully explored (Fig. 3C).

The 3-D magnetic susceptibility inversions (Fig. 4) show higher susceptibilities where known deposits are located and suggest approximate shapes, orientations, and relative extents. The deposit with the largest volume of high susceptibilities is the Barton Hill group ore body near Mineville (Fig. 3c, 4a), which extends at depth over a kilometer, consistent with published documentation.

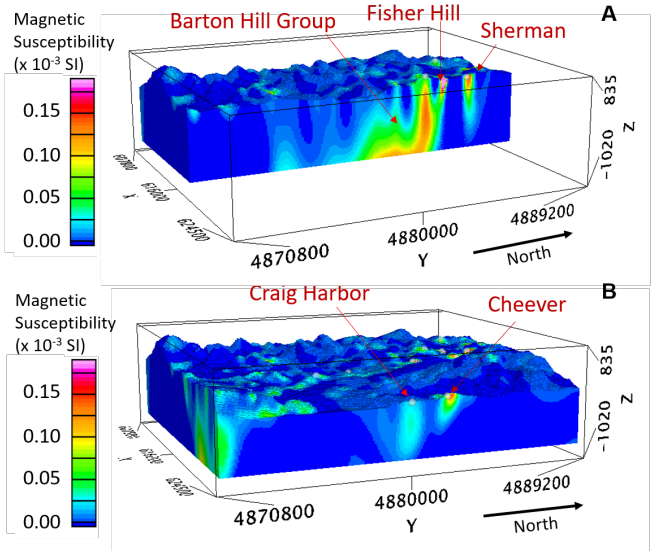

Figure 4. Vertical slices through the 3-D magnetic susceptibility model near the A) Barton Hill group in Mineville and B) the Cheever Mine. Dimensions in meters with 3x vertical exaggeration.

Other deposits such as at Cheever and Pilfershire are smaller but also south-plunging. Some deposits such as the Lou Smith prospect appear more vertical.

5 Discussion

The magnetic field highlights host rock and major structural features. A cursory consideration of the magnetic total field might suggest that individual deposits cannot be distinguished. However, application of high-pass filtering approaches can indeed highlight anom-alies associated with the magnetite-apatite deposits.

For this dataset we found that filters applied to flight line data were more effective than those applied to gridded data because narrower features can be highlighted. Care must be taken with these approaches, however, because isolated magnetic bodies can appear magnetically similar to the deposits. The 3-D models, which were applied to the total field, are also able to delineate magnetite deposits, along with their general shape, orientation and relative size.

The radiometric data show eTh-eU anomalies that outline tailings piles rich in REE-bearing apatite, reflecting a correlation between Th and REEs. Local eTh anomalies do not, however, delineate *in situ* REE-bearing deposits, perhaps because of tremendous local variability in apatite concentrations. The deposits do not show a correlation with radiometric K, probably because potassic alteration has been overprinted with sodic alteration over much of the area. These observations thus show important differences in the way alteration history can impact the geophysical expression of IOA deposits.

Acknowledgements

The code for the magnetic susceptibility inversions was written by J. Phillips; we are grateful for his help with implementation. Margaret Goldman, Anna Klein, and Cliff Taylor provided indispensable help in the field and in the laboratory. We thank Marian Lupulescu, Paul Tromblee, and Thomas Scozzafava for facilitating visits to some of the mine and/or tailings sites. We thank A. McCafferty and J. Austin for helpful reviews. This effort was funded by the USGS Mineral Resources Program.

References

Austin J, Foss C (2012) Rich, attractive and extremely dense: A geophysical review of Australian IOCGs. International Geophysical Conference and Exhibition, 22nd, Brisbane, Australia, Extended Abstracts

Chiarenzelli JR, Selleck B, Lupulescu M, Regan S, Bickford ME, Valley P, McLelland J (2017) Lyon Mountain ferroan leucogranite suite: Magmatic response to extensional thinning of overthickened crust in the core of the Grenville orogeny. Geol Soc of Amer Bull 129:1472–1488

Clark DA, Geuna S, Schmidt PW (2003) Predictive magnetic exploration models for porphyry, epithermal and iron oxide copper-gold deposits: Implications for exploration, exploration and mining. Commonwealth Scientific and Industrial Research Organization (CSIRO) Exploration and Mining Report 1073R

Direen NG, Lyons P (2007) Regional crustal setting of iron oxide Cu-Au mineral systems of the Olympic Dam region, South Australia: Insights from potential-field modeling. Econ Geol 102:1397–1414

Farrell P. (1996) Through the Light Hole, North Country Books, Utica, N.Y.

Foose MP, McLelland JM (1995) Proterozoic low-Ti iron-oxide deposits in New York and New Jersey: relation to Fe-oxide (Cu–U–Au–rare earth element) deposits and tectonic implications. Geology 23:665–668

Fraser D C, Fuller BD, Ward SH (1966) Some numerical techniques for application in mining exploration. Geophysics 31:1066–1077

Hayward N, Enkin RJ, Corriveau L, Montreuil J-F, Kerswill J (2013) The application of rapid potential field methods for the targeting of IOCG mineralisation based on physical property data, Great Bear magmatic zone, Canada. Journal of Applied Geophysics 94:42–58

Isachsen YW, Fisher DW (1970) Geologic map of New York: Adirondack sheet. New York State Museum Map and Chart Series 15, scale 1:250,000

Kemp JF (1898) The geology of the magnetites near Port Henry, N.Y. and especially those of Mineville. Transactions of the American Institute of Mining Engineers 27:147–203

Kemp JF, Ruedemann R (1910) Geology of the Elizabethtown and Port Henry Quadrangles. New York State Museum Bulletin 138, New York State Education Department

Lupulescu MV, Hughes JM, Chiarenzelli JR, Bailey DG (2017) Texture, crystal structure, and composition of fluorapatites from iron oxide-apatie (IOA) deposits, eastern Adirondack Mountains, New York. The Canadian Mineralogist, 55:399–417

Mariano AN, Mariano A (2012) Rare earth mining and exploration in North America. Elements 8:369–376

McCafferty AE, Phillips JD, Driscoll RL (2016) Magnetic and Gravity Gradiometry Framework for Mesoproterozoic Iron Oxide-Apatite and Iron Oxide-Copper-Gold Deposits, Southeast Missouri. Econ Geol 111:1859–1882

McKeown FA, Klemic H (1956) Rare-earth-bearing apatite at Mineville, Essex County, New York. U.S. Geological Survey Bulletin 1046-B

Phillips J (2014) Using vertical Fourier transforms to invert potential-field data to magnetization or density models in the presence of topography. Society of Exploration Geophysicists 2014 Technical Program Expanded Abstracts

Sandrin A, Elming SÅ (2006) Geophysical and petrophysical study of an iron oxide copper gold deposit in northern Sweden. Ore Geol Reviews 29:1-18

Sandrin A, Berggren R, Elming SÅ (2007) Geophysical targeting of Fe-oxide Cu–(Au) deposits west of Kiruna, Sweden. Journal of Applied Geophysics 61:92–101

Shah AK (2016) Airborne Geophysical Surveys over the Eastern Adirondacks, New York State. U.S. Geological Survey Data Release https://dx.doi.org/10.5066/F72R3PT0.

Shives RB, Charbonneau BW, Ford KL (2000) The detection of potassic alteration by gamma-ray spectrometry—Recognition of alteration related to mineralization. Geophysics 65:2001–2011

Smith RJ (2002) Geophysics of iron oxide copper-gold deposits, in Porter TM, ed., Hydrothermal iron oxide copper-gold and related deposits: A global perspective. Adelaide, PGC Publishing 2:357–367

Taylor RD, Walsh GJ, Taylor CD, Shah AK (2018a) Potential REE resources in mine waste, tailings piles, and iron oxide-apatite deposits of the eastern Adirondack Highlands, New York, USA. Metals, Minerals, and Society, SEG 2018, Keystone, Colorado

Taylor RD, Taylor CD, Walsh GJ, Shah AK (2018b) Geochemistry of ore, host rock, and mine waste pile samples of iron oxide-apatite (IOA) deposits of the eastern Adirondack Highlands, New York, in relation to potential rare earth elements resources, 2016-2018: U.S. Geological Survey Data Release, https://doi.org/10.5066/P9EEXCKI

Valley PM, Hanchar JM, Whitehouse MJ (2011) New insights on the evolution of the Lyon Mountain Granite and associated Kiruna-type magnetite-apatite deposits, Adirondack Mountains, New York State. Geosphere 7:357–389

New methodology of application of historical geophysical materials for the exploration of mineral deposits, as presented for the Nowa Sól area

Lidia Dziewińska
IGSMiE PAN, Cracow, Poland

Andrzej Pepel
S-Systems, Warsaw, Poland

Stanisław Speczik
University of Warsaw, Poland

Waldemar Jóźwiak, Krzysztof Zieliński
Miedzi Copper Corp., Warsaw, Poland

Abstract. The paper presents new methodology of adapting historical geophysical materials for the indication of prospective zones of Cu-Ag deposits, with the Nowa Sól exploration target in Poland used as an example. Basic gravimetric materials and transformed maps were combined to assess the tectonic structure of the region. The new method of effective reflection coefficients (ERC) allowed the application of archival seismic records for a more precise determination of the most vaguely traced interfaces within the Zechstein unit. Compared to an amplitude-based seismic section, an ERC section is characterised by its highly increased resolution of imaging.
Keywords: Fore-Sudetic Monocline, Nowa Sól exploration target, copper and silver deposits, geophysical data processing, effective reflection coefficients

1 Introduction

As the first stage of its exploration project in the Nowa Sól area, Miedzi Copper Corp. (MCC) performed extended analyses of existing historical geophysical materials. However, the quality of this abundant data did not allow its application for ore prospecting. Therefore, the use of new methods was necessary to trace the prospective zones of Cu-Ag mineralisation (Speczik et al., 2011, 2012; Dziewińska et al., 2017). The locations of prospecting boreholes were established after the reprocessing of geophysical data by means of the new methodology. The produced results compared to the effects of drilling confirmed the usefulness of the applied methodology.

2 Geological setting of the research area

The research area is located in Poland, in the south-western part of the Fore-Sudetic Monocline, on the southern slope of the Wolsztyn High. This region is interpreted as the eastern extension of the Rheno-Hercynian (RH) and Saxo-Thuringian (ST) zones demarcated within the Variscan orogen of Germany, as well as the Mid-German Crystalline Rise (MGCR) (Grad et al. 2016). In Poland and Germany, these units are associated with the occurrence of mineral deposits (Wyżykowski 1971; Rydzewski 1978; Franke et al. 1993; Cwojdziński et al. 1995; Żelaźniewicz et al. 1997; Oszczepalski 1999), which justifies the performance of prospecting work.

3 An overview of current geophysical knowledge

The role of tectonic movements and the associated magmatic and hydrothermal processes as a factor destabilising the palaeo-hydrological balance in ore formation process presents a direction for geophysical research. The Cu-Ag deposits being explored are categorised as epigenetic, created due to the migration of low-temperature hydrothermal solutions. Migration pathways probably included regional and local tectonic zones. Those fractures could be considered as channels for the convection of heat necessary for mineralising processes (Speczik 1985; Piestrzyński 2007). A semi-detailed seismic image prepared for the Nowa Sól area by petroleum companies in the years 1980-1994 constitutes a grid of profiles of varying quality, 1-2 km apart from each other. Main structural objects were identified in the prospective sediments of the Main Dolomite lithostratigraphic unit. Zones of changes in the record are related primarily to changes in the lithology, facies and thickness of Zechstein cyclothems, in particular Stassfurt and Werra, as well as the occurrence of tectonically deformed regions. Historical gravimetric surveys in the form of a semi-detailed image with the density of points of approximately 3.5 point/km^2 cover the whole area and its nearest surroundings. The values of anomalies are sufficient for a gravimetric study related to the rocks of Zechstein and its substrate. In terms of geology, the gravimetric image has visible high-density rocks of the older Palaeozoic or metamorphic rocks of the Wolsztyn-Pogorzela High (Kiersnowski et al. 2010). For

shallower depth intervals, the recorded residual anomalies reflect changes in the lithology and thickness of Zechstein sediments related to salts and anhydrites of varying density. The densities of P1 sediments range from 2.55 to 2.65 g/cm^3. Due to their position and structure, Triassic rocks distinguished by densities exceeding 2.5 g/cm^3 have no significant impact on the recorded gravimetric image. Various transformations of the image used the methods of analogue and frequency-based filtration. Along with an analysis of zones with increased gradients, this allowed tracing geological objects with elongated shapes, like faults or anticlines, as well as facial changes within analysed depth intervals. A horizontal gradient map (Figure 1) presents a zone of anomalies with a NW-SE direction, approximately parallel to the Wolsztyn High, probably indicating a tectonic zone located close to its south-western limb. The deep origins of this zone are confirmed by magnetic data and the results of seismic refraction (Dziewińska et al. 2017).

4 The methodology of processing ERC seismic sections

The principles of the effective coefficient method known back then as “Reapak” were developed in “Sibgeo Novosibirsk” in the 1980s (Rudnitskaya et al. 1987). This method was modified and adjusted to the lithological and tectonic variability of Zechstein sediments by the authors of the present paper (Speczik et al. 2011). The calculations used materials prepared by the petroleum industry based on historical seismic data (time records, seismic sections) retaining their original amplitudes.

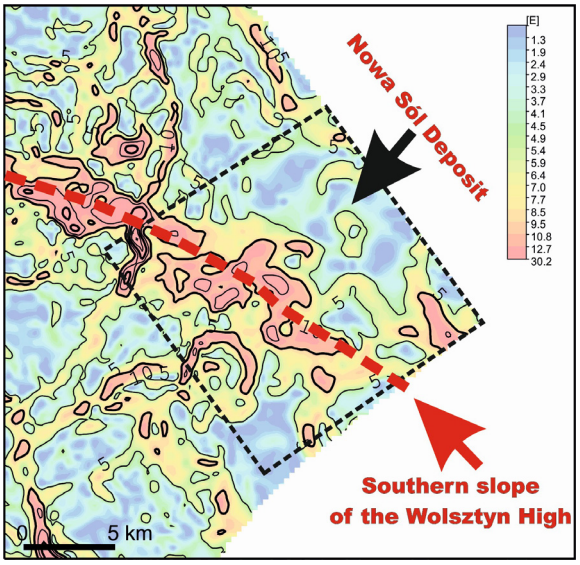

Figure 1. A horizontal gradient map according to Rosenbach.

The calculation of effective reflection coefficients (ERC) enables the conversion of a waveform seismic image into an impulse form of seismic record, meaning a temporal sequence of reflection coefficients presenting the subsequent layers forming a given geological structure. To this end, one of the most important features of a seismic image is used – the amplitude, its size being assumed as proportional to the reflection coefficient for a specific geological boundary. The mathematical and physical model of a geological structure is a so-called convoluted model, according to which a seismic pathway is the result of combining the pathway of refection coefficients with elementary seismic signal. The deconvolution of an amplitude-based seismic pathway allows obtaining a seismic pathway in the form of a series of coefficients. Processing pattern includes three stages: determination of an elementary impulse, repeated mutual correlation of the impulse with the seismic pathway, as well as standardisation (horizontal and vertical addition of the individual pathways) and the use of a statistical report for the visualisation of a seismic image. The primary function of the system involves determining the shape of the elementary signal and establishing the impulse characteristics of the structure. The determination of an elementary seismic impulse proceeds by the addition of subsequent groups of reflected waves for the given pathway, presented for the same phase, and the combined time of recording. Results of the determination of elementary signal can be validated using Fourier analysis. The function of mutual correlation of elementary signal with each seismic pathway enables conversion of a wave-based seismic pathway into temporal series of zero-phase amplitudes called the effective reflection coefficients. It determines the time-based points of maximum correlation of signal with reflected waves in the form of values of the coefficient and sign of the amplitude. Sets of reflection coefficients undergo standardisation and they are presented in the form of a seismic section which shows seismic pathways converted into an impulse form. The reflection coefficients present seismic interfaces conforming to actual boundaries. This coefficient is defined by layer-related velocities and rock density above and below a given seismic reflecting interface. Assuming that changes in density are relatively small compared to changes in velocity, it is accepted that the coefficient depends mainly on the latter. This method is particularly useful when identifying thin layers, small dislocations, and tracing changes in the lithology of a given stratum, e.g. porosity, along a seismic section. Geophysical logging performed in boreholes enabled calculations of the values of parameters for strata exceeding 4 m in thickness. The values of density in individual stratigraphic units enable the construction of one averaged density model of an area. Due to the use of the attributes of an impulse section and the sign of the reflection coefficient, reflected wave intensity and the place of reflection, the efficiency of identification and correlation of seismic boundaries increases, along with simultaneous characterisation of the geometrical and physical system of strata forming a given geological structure. Evaluation of the properties of the ERC method is facilitated by comparing section TA220782 developed as reflection coefficients (Figure 2) to a fragment of its unprocessed version (Figure 2-A).

5 The analysis and interpretation of ERC sections for predicting ore distribution

The analysis and interpretation of results covered 9 selected seismic profiles: T0970783, TA220782, T0190790, 115-04-93K, 106-04-93K, 107-04-93K, 118-04-93K, 114-4-93K and TA230782 (Figure 3) with a total length of 82.233 km.

The ultimate objective was to demarcate the probable zones of increased thickness of potential ore-bearing series. One characteristic feature is the arrangement of coefficients and zones of particular significance for predicting the occurrence of copper-bearing shales and the associated mineralised zones with the highest possible probability.

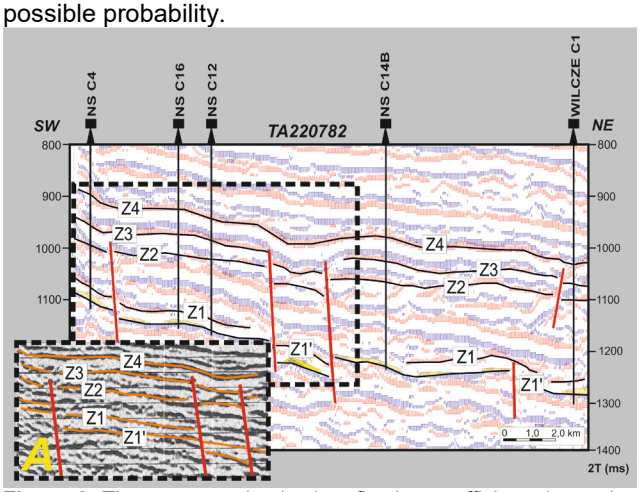

Figure 2. Time-converted seismic reflection coefficients in section TA220782 of a Zechstein deposit compared to an amplitude section (A).

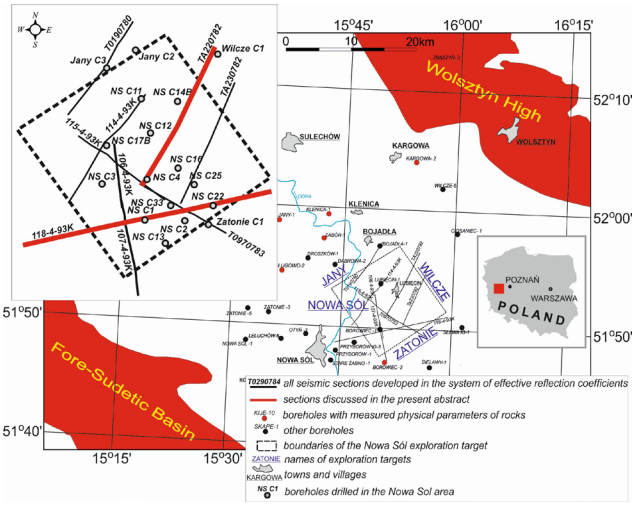

Figure 3. Location map.

On the seismic sections, particular attention was paid to the position of the boundary between Z1' and Z1. Identification of the traced stratigraphic horizons: Z4, Z3, Z2, Z1 and Z1' (see Figure 4) is analogical to what is used traditionally in the Fore-Sudetic Monocline. The nature and magnitude of reflection coefficients indicate that Zechstein sediments may be underlain by insets of rocks characterised by much higher velocity compared to sandstones. Fault zones in horizon Z1' are associated with the diverse morphology of sub-Zechstein sediments. Most faults recorded in the Zechstein extend into older rocks, evidencing their deeper tectonic origins. Zechstein sediments stand out on ERC sections due to boundaries with high values of the coefficients, documenting great lithological diversity of rocks which form series of salts, clays, as well as anhydrites and dolomites. Observed changes in the thickness of complexes between these horizons are caused mainly by changes in the thickness of the older salt of the Stassfurt cyclothem and the oldest salt and anhydrite of the Werra cyclothem.

6 Usefulness of the ERC method applied for establishing the location of boreholes

Zones of lithological changes with characteristic values of the coefficients and low-amplitude faults have been recorded within Zechstein rocks and along their contact with the Rotliegend. In the Zechstein complex Z1'-Z1, there are visible interfaces originating from its individual strata. Particularly noticeable is a high-velocity complex of Zechstein sediments directly above the top of the Rotliegend. An assumption was made about the connection between the bottom part of the complex characterised by the Z'1 reflective interface and the geological objective, as well as possible changes in the coefficients recorded above the Z'1 boundary. Drilling results indicate that rocks associated with the orebody are several metres thick, and physical parameters characterising these sediments: velocity, density and porosity, have values similar to the highly elastic thick structure present in their overburden, consisting of limestones, anhydrites and rock salts. The presented image justified the particular attention paid to the interpretation of ERC sections for correlation between a negative reflection coefficient associated with the base of Zechstein and changes in the shape of a system of reflection coefficients present above it. Based on the arrangement of reflection coefficients, a graphical representation has been shown involving the shape of characteristic strata in the vicinity of the contact of Zechstein and Rotliegend, which are believed to be prospective in the studied area. Changes in the lithology of lowermost Zechstein sediments (interlayers and various insets) occur above the Z1' seismic boundary as reflections with low values of the coefficients recorded in short segments of the profiles. They have been interpreted as “anomalous strata”, indicating the sites of potential mineralised zones.

Section 118-4-93K with a nearly latitudinal direction (Figure 4) is the most representative of all seismic sections selected for reprocessing. Along the Przyborów elevation and on its eastern slope, several anomalous zones were recorded at the boundary between the Zechstein and the Rotliegend, which due to the discontinuity of correlation were linked with Cu ore. Section TA220782 (Figure 2) presents an undisturbed position of seismic interfaces dipping towards the NE. The interpreted potential orebodies are situated at the SW and NE ends of the section, in the central part of the

profile between two discontinuities delimiting a depression in the Zechstein horizon.

7 Summary and conclusions

The transformation of archival seismic data into effective reflection coefficients (ERC) enabled the demarcation of Z1'-Z4 interfaces in Zechstein rocks. It also allowed the identification of tectonic features and the characteristic zones of lithological changes near the Z1' interface, which are possible hosts to orebodies. The presented assumptions and possibilities of depicting changes in mineralised zones along ERC sections have provided information about characteristic places associated with potential orebodies. These sections enabled the indication of more precise locations for planned prospecting boreholes.

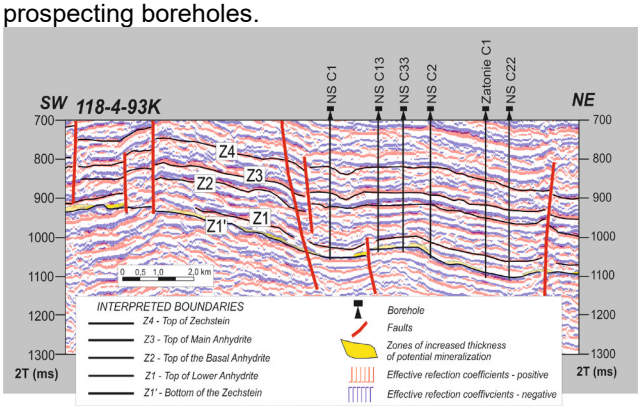

Figure 4. Time-converted seismic reflection coefficients in section 118-4-93K of a Zechstein deposit.

Table 1. Efficiency of the used ERC method.

Borehole	Correlation with ERC image	Seismic section
NS C1	YES	118-4-93K, 106-4-93K
NS C2	YES	118-4-93K, T0970783
NS C3	NO	118-4-93K, T0970783
NS C4	YES	TA220782, 115-4-93K
NS C11	NO	114-4-93K
NS C12	NO	TA220782, 114-4-93K
NS C13	YES	118-4-93K, 107-4-93K
NS C14B	YES	TA220782
NS C16	YES	TA220782, TA230782
NS C17B	YES	115-4-93K, 114-4-93K, 106-4-93K
NS C22	YES	118-4-93K, T0970783
NS C33	YES	118-4-93K, T0970783

Borehole C17B described as negative reflects the lack of characteristic anomalies associated with potential mineral series on three interpreted ERC sections. Summarising the produced results, for twelve prospective boreholes drilled, nine remain in compliance with the ERC image and three (C3, C11, C12) present a negative result of correlation. This proves the high validity of the performed interpretation of seismic sections in relation to drilling results and justifies the adopted course of research. Boreholes drilled close to or along the interpreted seismic sections confirmed the effectiveness of the ERC method in approximately 75%. Prospective boreholes planned near the slope of a zone of higher gradients in the substrate of Zechstein proved to be located properly in terms of suggested relationship of mineralised zones with Zechstein base morphology. The completed drilling operations also confirmed the assumption about the position of lower Zechstein copper orebodies, forming a rather wide strip (5-10 km) placed in a zone extending NW-SE along the eastern range of the Zielona Góra oxidised area (Zieliński and Speczik 2017). The presented results have been produced based on historical documentation, with relatively low financial expenses and with no need for costly on-site work. This study also has a methodical nature, showing the ability to use the impulse form of a seismic record for the identification of prognostic Cu and Ag resources, as confirmed by the results of prospecting drilling.

References

Cwojdziński S., Młynarski S., Dziewińska L., Jóźwiak W., Zientara P., Baziuk T. (1995) Pierwszy sejsmiczny profil głębokich badań refleksyjnych (GBS) na Dolnym Śląsku. Przegląd Geologiczny, 43:727-737.

Dziewińska L., Pepel A., Tarkowski R., Żuk Z. (2017) Nowe spojrzenie na wyniki badań geofizycznych monokliny przedsudeckiej w aspekcie poszukiwań surowców mineralnych. Biuletyn Państwowego Instytutu Geologicznego, 468:165-174.

Franke W., Żelaźniewicz A., Porębski S.J., Wajsprych B. (1993) The Saxothuringian zone in Germany and Poland: differences and common features. Geologische Rundschau, 82:583-599.

Grad M., Polkowski M., Ostaficzuk S.R. (2016) High-resolution 3D seismic model of the crustal and uppermost mantle structure in Poland. Tectonophysics, 666:188-210.

Kiersnowski H., Peryt T.M., Buniak A., Mikołajewski Z. (2010) From the intra-desert ridges to the marine carbonate island chain: middle to late Permian (Upper Rotliegend – Lower Zechstein) of the Wolsztyn–Pogorzela high, west Poland. Geological Journal, 44:319-335.

Oszczepalski S. (1999) Orgin of the Kupferschiefer polymetallic mineralization in Poland. Mineralium Deposita, 34(5): 599-613.

Piestrzyński A. (2007) Historyczny rozwój poglądów na genezę złoża rud miedzi na monoklinie przedsudeckiej - dyskusja. Biuletyn Państwowego Instytutu Geologicznego, 423:69-76.

Rudnitskaya D.I., Danenberg E.E., Belozerov V.B. (1987) Principy vydelenija sejsmociklitov v kontinentalnyh otlozhenijah jury Zapadno-Sibirskoj plity v svjazi s poiskami neantiklinalnyh zalezhej nefti i gaza. In: Prikladnye voprosy sedimentacionnoj ciklichnosti i neftegazonosnosti. Novosybirsk-Nauka, 67-72.

Rydzewski A., (1978) Facja utleniona cechsztyńskiego łupku miedzionośnego na obszarze monokliny przedsudeckiej. Przegląd Geologiczny, 26(2):102-107.

Speczik S. (1985) Metalogeneza podłoża podcechsztyńskiego monokliny przedsudeckiej. Geologica Sudetica, 20:37-96.

Speczik S., Dziewińska L., Pepel A., Jóźwiak W. (2011) Możliwość wykorzystania impulsowej postaci zapisu sejsmicznego do rozpoznania złóż prognostycznych miedzi i srebra w północnej części monokliny przedsudeckiej. Zeszyty Naukowe IGSMIE-PAN, 81:117-135.

Speczik S., Dziewińska L., Pepel A., Jóźwiak W. (2012) Analiza i przetwarzanie danych geofizycznych, jako instrument poszukiwań złóż z Cu-Ag na monoklinie przedsudeckiej. Biuletyn Państwowego Instytutu Geologicznego, 452:257-286.

Wyżykowski J. (1971) Cechsztyńska formacja miedzionośna w Polsce. Przegląd Geologiczny, 19(3):117-122.

Zieliński K., Speczik S. (2017) Głębokie złoża miedzi i srebra szansą dla górnictwa metali w Polsce. Biuletyn Państwowego Instytutu Geologicznego, 468:153-164.

Żelaźniewicz A., Cwojdziński S., England R.W., Zientara P. (1997) Variscides in the Sudetes and the reworked Cadomian orogen: evidence from the GB-2A seismic reflection profiling in southwestern Poland. Geological Quarterly, 41(3) 289-30.

Implicit model creation for the application of geophysical inversion and forward modelling; drill target generation for undercover ore deposits

Daniel Gerger, Patrick Ledru, Dwayne Kinar, Grant Harrison
Orano Canada Inc., Saskatoon, Canada

Gabriel Courrioux
BRGM, Orléans, France

Charles Gumiaux
University of Orléans, ISTO, Orléans, France

Abstract. Exploration for undiscovered uranium deposits within the Athabasca Basin, Saskatchewan, Canada is complicated by a thick sedimentary cover, masking the geophysical expression of the basement-sandstone unconformity interface that provides a favourable pathway and trap for mineralizing fluids. Zonal alteration associated with uranium deposition disrupting the regional distribution law of density and resistivity must be identified and parsed from the primary controls on the geophysical response; geological and structural form of the underlying strata. Provided a solid understanding of the geological context, these secondary disruptions can be identified and targeted for diamond drilling investigation through inversion processing of the geologic model.

A 3D block model of an exploration zone has been created through implicit modelling from sparse drill-hole data to aid in three-dimensional visualization, inversion modelling and resulting target optimization. When combined with an 'expert-driven' approach to data analysis regarding principal metallogenic guides within the geological context of the exploration area, identification of zones of physical property variation unaccounted for in the primary geological conditions can be used to vector towards zones of interest for improved drill targeting of deeply buried ore deposits.

1 Introduction

The advancement of successful geoscience targeting in an efficient manner continues to become more difficult as near-surface deposits that can be easily identified are increasingly rare to discover. This is true across most mineral commodities and is particularly significant for high-grade uranium deposits endemic to the Athabasca basin in northern Saskatchewan, Canada. Recent discoveries in the most explored districts, with a few exceptions, are confined to several hundred metres below the topographic surface and as such are termed "blind" deposits due to the nature of the technically difficult exploration that must be undertaken. Application of geophysical methods reconciled with known geological constraints can aid in the reduction of uncertainty inherently associated with exploration at depth.

The Athabasca basin is a district of significant economic interest as it is known to host many of the world's largest and highest-grade uranium deposits (Card et al. 2007). The metallogenic model follows the precipitation of uranium in the form of pitchblende or uraninite during low-mid temperature redox reactions at the discordant contact between Archean to Paleoproterozoic metamorphic basement gneisses and the Paleoproterozoic Athabasca sedimentary sequence (Jefferson et al. 2007). Deposit formation is typically associated with steeply dipping, structurally re-activated shear zones acting as fluid flow conduits within high metamorphic grade, graphite-bearing paragneisses. Graphitic horizons are identified through electro-magnetic (EM) geophysical methods and have historically been used as a first-order exploration guide. As graphitic horizons are wide-spread across the basement of the Athabasca basin, various other geophysical methods can be used to infer the changes in the spatial distribution of physical rock properties that may be indicative of uranium precipitation, to help narrow down areas of exploration interest. The most utilized methods apart from EM include DC resistivity, magnetics, and gravity. Alteration associated with uranium deposition is hydrothermal; generally argillic to propylitic in nature and as such significantly reduces the density and resistivity of the country rock (Hoeve and Quirt 1984; Quirt 2003).

This study focuses on the effects of density variation as it pertains to the gravity response across known areas of alteration within a uranium exploration project, Getty Russell, operated by Orano Canada Inc. in partnership with Cameco Corporation, along the Wollaston-Mudjatik Transition Zone in the Athabasca basin (Fig. 1). Using the 3D Geomodeller (Intrepid) software, a 3D block model has been created within the exploration project area with the goals of better imaging the structural geometry of the basement geology, mapping known alteration corridors, and using geophysical inversion methodology to identify areas of anomalous petrophysical property variations that could be associated with alteration. The geophysical signature will be dominantly controlled by the geology and structure of the underlying strata and consequently alteration zones act as discreet and difficult to determine

contributions. These alteration zones must be considered as secondary effects on the overall geophysical response that can be quantified through the inversion workflow.

Identification of areas of physical property variation not currently accounted for within the geological model, which may be related to alteration haloes associated with uranium mineralization, facilitates exploration by concentrating efforts towards zones with the highest potential prospectivity. Diamond drilling is an expensive but necessary method of exploration for buried ore deposits (Doney et al. 2015); through cross-validation and reconciliation of all available data, innovative approaches can be developed to lessen this expense and better focus exploratory efforts.

2 Methodology

For the most consistent elimination of ambiguity and to decrease uncertainty as much as possible within the original 3D geological model before inversion processing, data associated with the original model must be interpreted and cleaned as much as possible (Gerger 2018). Comprehension and simplification of heterogeneous geological units, examination of regional alteration that will have an effect on gravity modelling, examination of the available geophysical data and its use and integration in geological interpretation, application of GIS tools that can aid in the modelling process, and assumptions made going forward with regional scale 3D models, including geological, structural, and geophysical criteria must all be reconciled to create a stepwise approach to this case study:

1) Construction of an unconformity plan geology map respecting all available geophysical interpretations, project geological data and interpretation, and drill-hole constraints.

2) Define a stratigraphic pile in Geomodeller that is reflective of the stratigraphic relationships between present lithologies (Calcagno et al. 2008). The interpolation is dependent upon the choices made with respect to these interpreted relationships and therefore all observed field relationships between differing rock layers must be considered.

3) Import drill-hole constraints to the Geomodeller database after simplification to make the logged geology comprehendible at a regional scale. Respect contacts, generalized lithologies, and orientation data where available. Adjust and re-interpolate the model based on drill-hole importation and/or update with drilling progress and new information.

4) Create regional and grid scale cross-sections orthogonal to geology and structure in order to assess behaviour of the model at depth. Use existing cross-sections and orientation data to add constraints to the shape and trend of interpolated geology.

5) Introduce alteration envelopes into the model and discretize based on the parent lithologies overlapped by the alteration (Fig. 2).

6) Analyze and input physical property data into the different units of the 3D model, constructing a density block of the petrophysical property distribution across the project area. Statistical distribution of the density loss due to alteration must originate from field information (Fig. 3).

7) Forward model the response of the 3D geological model iteratively throughout the modelling process. Correct and reconcile to obtain a best-fit for the observed potential fields.

8) Continue with inversion modelling in Geomodeller to obtain areas of exploration interest not currently accounted for by the distribution of physical properties across the geological block model.

This process requires a significant amount of data to be used from a variety of sources. The most relevant sources are: digital terrain map of the project area, magnetics maps, gravity surveys (Fig. 4a), EM surveys, logged geology, geochemical data, interpreted unconformity map, historical interpretations of the area (Annesley et al. 2005; Tran 2006; Jeanneret et al. 2016), drill-hole intersections, and petrophysical property data. Forward modelling is the critical step to create a reasonable block model before going forward with inversion and target acquisition.

3 Forward and inversion modelling to characterize and target alteration zones

3.1 Alteration characterization

Forward modelling of known drilling intersected alteration zones is used to characterize the overall effect of uranium associated density loss on the gravity potential field (Fig. 4). Using the generalized alteration envelope (200 x 1500 x 400 m) it is apparent that for an alteration corridor of the approximately necessary size for an economic uranium deposit, the gravimetric response will be in the order of 0.4 mGal. The overall range of gravimetric values for the vertical gradient in the observed geophysical response is ~3.9 mGal. Using the assumption that the larger effect of the main alteration envelope (C2 alteration corridor, Fig. 4c) is under-represented in the geological model as it is solely constrained by drilling, it can be said that the effect of a large alteration corridor might represent a 10% effect on the overall gravity response in this particular geological setting. Through this workflow it is evident that the effect of a large alteration zone is discreet when several hundred metres from surface and that it acts as a secondary contributor to the overall geophysical response. Therefore, the identification of unknown zones of alteration could be aided by geophysical inversion as many discreet alteration bodies will be difficult to distinguish from the bulk gravimetric response by eye alone.

3.2 Inversion modelling for target advancement

Inversion modelling across the geological model has been carried out using both lithology inversion and density inversion workflows that allow the inversion to change the lithology or the density, respectively, to best fit the observed gravimetric response. An understanding of the geological and structural conditions associated with

uranium mineralization in the Athabasca basin such as graphitic metasediments, reactivated basement structures, and their intersections at the unconformity surface must be kept in mind when analyzing which areas of low density are the most interesting from a targeting perspective. Historic metallogenic guides across the eastern Athabasca basin indicate the importance of graphitic horizons and metasediments for uranium deposition. The inversion has therefore to be limited to add or change alteration only in the vicinity of prospective lithologies, leaving the remainder of the block model static. The effect of a large basement alteration zone is discreet at the depth of the unconformity-basement interface. However, through processing and knowledge-based analysis target areas can be identified.

This type of 'expert-driven' approach to analysis of the inversion results with respect to the accepted metallogenic guides can aid in vectoring towards zones indicative of possible low-density anomalies in the subsurface currently unaccounted for in the geological model (Fig. 5). The Getty Russell project area primarily targets basement mineralization as the dominant mineralization style intersected to date is of the 'ingress-type'. Therefore, efforts have been concentrated on the basement intersection with characteristic narrow alteration corridors.

4 Perspectives and conclusion

Results from the attempts to model and reconcile the project scale geology with the geophysical response indicate that through successive stages of workflow, difficult buried terrains can be modelled with reasonable results. Uranium exploration concentrated along defined graphite-bearing corridors significantly narrows the areas of interest while searching for anomalies in the results of the density inversion. This particular research has focused on uranium exploration set under the cover of several hundred meters of sandstone and Quaternary sediment cover (Ramaekers et al. 2007); however, this methodology could be applied to any type of sub-surface mineral deposit that has associated hydrothermal or propylitic alteration haloes that affect the density of the surrounding strata. Through the interdisciplinary approach looking at available geophysical, geological, geochemical, and spectral data sources, complications can be limited, yet room for advancement in the detail and scale of methodology remains.

Obvious gravimetric anomalies can be used as control zones to determine validity of the model and inversion. Density variations shown in the inversion can however be re-joined to the geological model and target areas identified from zones less characterized by historical drilling.

This workflow through forward modelling and inversion processing works based on the assumption that the first-order controls on the geophysical response of the project area are based on the geological and structural form of the underlying strata. Through geological modelling it can be demonstrated that hydrothermal alteration haloes can be contributing effects to the overall gravimetric response, yet are minor in comparison to the overall effect caused by the base geology and structure. Forward and inversion reconciliation between the predicted geological model based on field observations and the observed geophysical response can help to vector towards these discreet zones of physical property variation potentially associated with low-density alteration corridors.

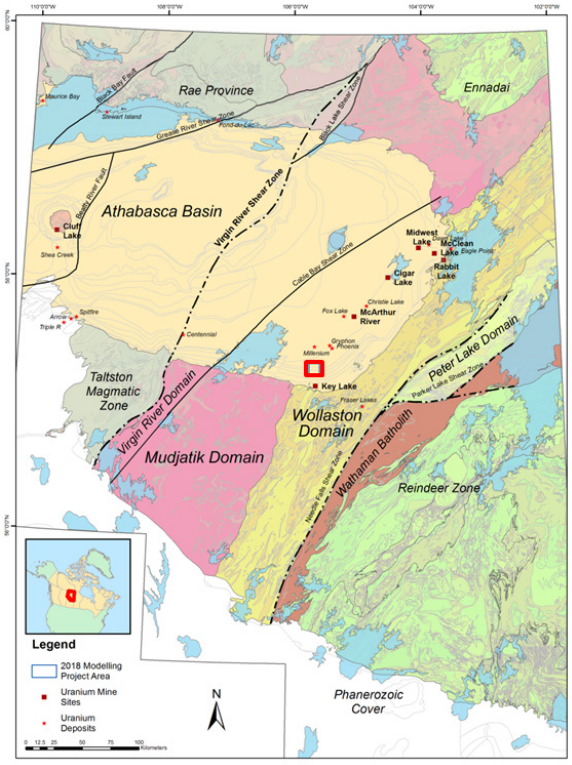

Figure 1. Project location map along the Wollaston-Mudjatik Transition Zone, Saskatchewan, Canada. The red rectangle highlights the 3D model location.

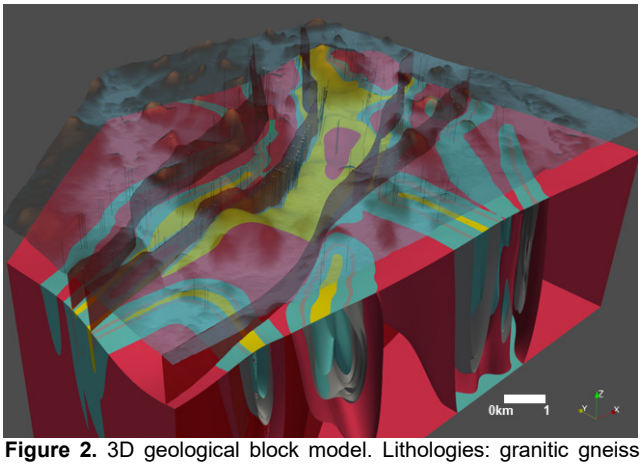

Figure 2. 3D geological block model. Lithologies: granitic gneiss (red); silicified gneiss (yellow); graphitic metasediments (grey); alteration zones (green); pelitic metasediments (blue). Vertical exaggeration x4.

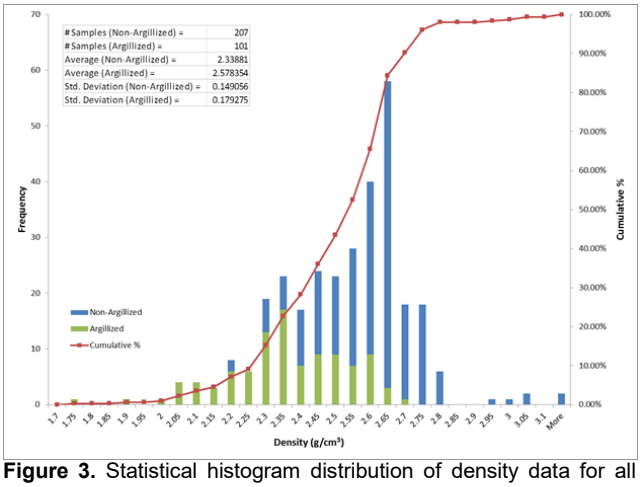

Figure 3. Statistical histogram distribution of density data for all basement lithologies. Blue represents unaltered lithologies; green represents logged alteration.

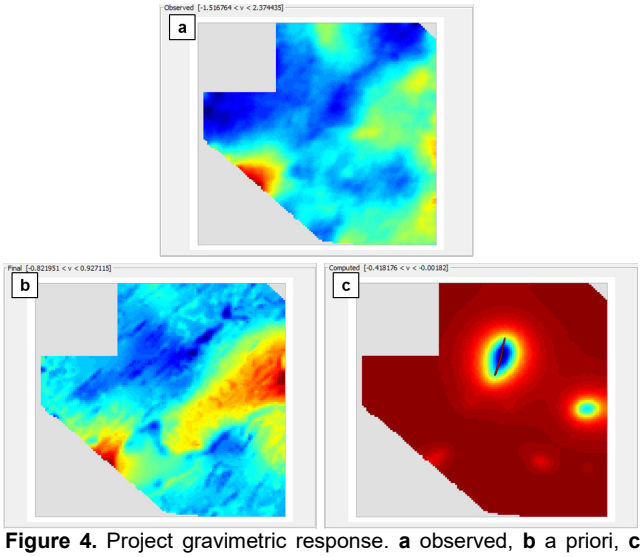

Figure 4. Project gravimetric response. **a** observed, **b** a priori, **c** individual contribution of the largest alteration zone intersected within the project boundaries.

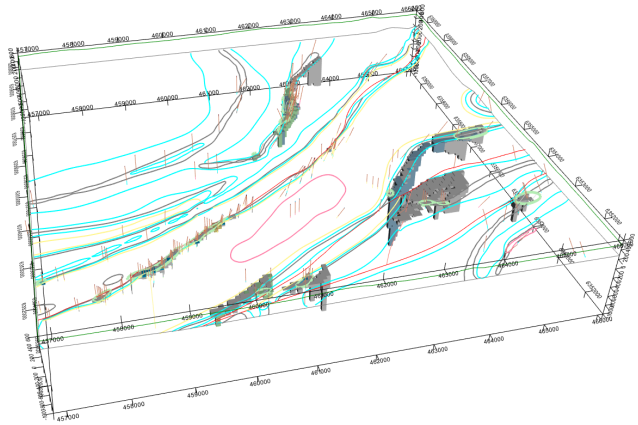

Figure 5. Queried alteration voxets showing inversion-predicted alteration zones. Coloured lines indicated lithological boundaries at the unconformity surface.

References

Annesley IR, Madore C, Portella P (2005) Geology and thermotectonic evolution of the western margin of the Trans-Hudson Orogen: evidence from the eastern sub-Athabasca basement, Saskatchewan. Can J Earth Sci 42: 573-597

Calcagno P, Chilès JP, Courrioux G, Guillen A (2008) Geological modelling from field data and geological knowledge Part I. Modelling method coupling 3D potential-field interpolation and geological rules. Physics of the Earth and Planetary Interiors 171: 147-157

Card CD, Pana D, Portella P, Thomas D, Annesley IR (2007) Basement rocks to the Athabasca Basin, Saskatchewan and Alberta. In: Jefferson CW, Delaney G (eds) EXTECH IV: Geology and Uranium EXploration TECHnology of the Proterozoic Athabasca Basin, Saskatchewan and Alberta; Geol Surv of Canada, Bull 588: 69-87

Doney A, Kinar D, Hutchinson R, Anderson M, Richard Y (2015) Reconciling Geology and EM Response in Unconformity Uranium Deposit Exploration: Examples from the Eastern Athabasca, Canada. 13th SGA Biennial Meeting 2015. Proceedings, Vol 5: 1797-1800

Gerger D, (2018) Implicit model creation for the application of geophysical inversion and forward modelling; drill target generation for undercover ore deposits. MSc Thesis. Université d'Orléans.

Hoeve J, Quirt DH (1984) Mineralization and host rock alteration in relation to clay mineral diagenesis and evolution of the Middle-Proterozoic Athabasca Basin, Northern Saskatchewan, Canada. Sask Res Council, Pub R-855-2-B-84

Jeanneret P, Goncalves P, Durand C, Trap P, Marquer D, Quirt D, Ledru P (2016) Tectono-metamorphic evolution of the pre-Athabasca basement within the Wollaston-Mudjatik Transition Zone, Saskatchewan. Can J Earth Sci 53: 231-259

Jefferson CW, Thomas DJ, Gandhi SS, Ramaekers P, Delaney G, Brisbin D, Cutts C, Portella P, Olson RA (2007) Unconformity-associated uranium deposits of the Athabasca Basin, In: Jefferson CW, Delaney G (eds) EXTECH IV: Geology and Uranium EXploration TECHnology of the Proterozoic Athabasca Basin, Saskatchewan and Alberta; Geol Surv of Canada, Bull 588: 23-67

Quirt DH (2003) Athabasca unconformity-type uranium deposits: One deposit type with many variations. In: Cuney M (ed) Uranium Geochemistry. International Conference Proceedings, Nancy 2003: 309-312

Ramaekers P, Jefferson C, Yeo G, Collier B, Long D, Drever G, McHardy S, Jiricka D, Cutts C, Wheatley K, Catuneanu O, Bernier S, Kupsch B, Post R (2007) Revised geological map and stratigraphy of the Athabasca Group, Saskatchewan and Alberta. In: Jefferson CW, Delaney G (eds) EXTECH IV: Geology and Uranium EXploration TECHnology of the Proterozoic Athabasca Basin, Saskatchewan and Alberta; Geol Surv of Canada, Bull 588: 155-191

Tran HT (2006) A preliminary Report on a visit to the Key Lake road Uranium property. Internal Report for Forum Uranium Corp.

Prospecting strategy for deep sediment-hosted Cu-Ag ore deposits in Poland

Stanisław Speczik, Tomasz Bieńko, Alicja Pietrzela
Miedzi Copper Corp., Al., Poland
University of Warsaw, Faculty of Geology, Poland

Krzysztof Zieliński
Miedzi Copper Corp., Al., Poland

Abstract. In 2011, Miedzi Copper Corp. initiated an exploration programme focused on deep Cu-Ag deposits in the Fore-Sudetic Monocline. The exploration target initially comprised 21 concessions. Their boundaries were based on known prognostic areas in the vicinity of palaeo-elevations and contacts between oxidised and reduced facies. During the first stage of the exploration programme, historical drill cores were analysed and samples were collected for further examinations, including organic geochemistry and the Rock Eval method. In some regions it revealed so-called strong Rote Fäule, a facies usually associated with high grade copper mineralisation. Also, geophysical data reprocessing was performed using an innovative method of effective reflection coefficients. Due to the results of this stage, the number of concessions was reduced in order to focus on the most promising areas. The drilling programme started in 2013. After its initial results, the operations continued in 6 concessions with the highest grade of ore. The exploration programme has led to the discovery of three deep Cu-Ag deposits in the Fore-Sudetic Monocline: Mozów, Sulmierzyce and Nowa Sól. The performed economic analyses proved that profitable mining operations in all three deposits are possible using modern extraction technologies.

1 Introduction

Copper supply from easily accessible deposits is recently decreasing due to the depletion of shallow, high grade reserves, both in porphyry and sediment-hosted deposit types, and due to the growing costs of copper extraction (Zieliński and Speczik 2017). Moreover, technological progress enables major companies to perform successful mining operations at greater depths (Addison et al. 2012, Zieliński et al. 2017). With growing demand for copper, it is much more justified to extract higher grade ore from deeper deposits, than lower grade ore from the shallower ones. For that reason, the exploration begins to target deeper mineralisation which in the near future will be a subject of economically reasonable extraction.

Therefore, in 2011 Miedzi Copper Corp. started a greenfield exploration programme in the northern part of the Fore-Sudetic Monocline in SW Poland. Copper-silver deposits in this region are of the stratiform sediment-hosted type, occurring in a contact zone between the continental red beds (Rotliegend) and Zechstein marine sediments. The ore-bearing series consists of white sandstones (Weissliegend), Kupferschiefer shales and Zechstein limestones (Oszczepalski 1989). The central part of the Fore-Sudetic Monocline is a well-known mining area (the Legnica-Głogów Copper District) where operations focused on deposits at depths between 700 and 1000 metres below ground level. However, deeper Cu-Ag mineralisation, occurring up to 1300 meters below ground level, have recently become a subject of interest. Miedzi Copper Corp. is focusing its exploration programme on targets where the ore occurs deeper than 1500 metres, with the potential for future extraction of rich deposits (Speczik et al. 2013; Zieliński et al. 2017).

2 Assumptions of the exploration project

The occurrence of Cu-Ag ore in deep parts of the Fore-Sudetic Monocline was noted for the first time in 1956; however, at this time the possibility of its development was not considered. Further investigation based on the re-examination of core samples and drilling data from deep oil and gas wells ultimately allowed the demarcation of Cu-Ag prognostic areas within deep parts of the Fore-Sudetic Monocline (Oszczepalski and Speczik 2011; Oszczepalski et al. 2012).

Miedzi Copper Corp.'s programme was focused on deep parts of the Fore-Sudetic Monocline, which had not previously been an object of interest of other companies (Zieliński et al. 2017). In 2011, Polish Ministry of Environment granted the company 21 prospecting concessions on the Fore-Sudetic Monocline. The concessions were selected based on several criteria, most importantly the vicinity of Permian palaeo-elevations (Wolsztyn and Szprotawa domes) surrounded by contacts between oxidised and reduced facies. High grade copper mineralisation is very likely to occur in places where transgressive, epigenetic and oxidising Rote Fäule facies contacts reduced sediments (Oszczepalski and Rydzewski 1997; Pieczonka et al. 2007). The areas with prognostic copper mineralisation demarcated by the Polish Geological Institute (Oszczepalski and Speczik 2011) were also considered while establishing the boundaries of exploration targets.

3 Investigation of historical data and geological materials

The first stage of Miedzi Copper Corp.'s exploration programme involved the examination of historical drill

core samples. These studies were carried out in core repositories of the National Geological Archive and PGNiG – Polish oil and gas company, and included the review of rock material from a total of 411 boreholes. Samples from 216 selected boreholes were a subject of extensive laboratory examination. Miedzi Copper Corp. collected 2559 samples for lithogeochemistry analyses and 1081 samples for petrological and mineralogical studies, with simultaneous examination of organic matter geochemistry. This constituted the first research-based determination of future copper and silver drilling targets in deep parts of the Fore-Sudetic Monocline.

In addition, the company performed the reprocessing of geophysical data, which involved examining 24 000 gravimetric points and more than 1700 km of seismic sections. Seismic data was reprocessed using the method of effective reflection coefficients (Speczik et al. 2012). It allows transforming a conventional seismic image into an impulse form of seismic records, meaning a temporal sequence of coefficients, whose sections can be correlated with the logs of historical boreholes in order to trace the course of lithological series. This method is useful for establishing the location of major structural features like faults, which are the crucial components of a mineralising system. The identification of certain major tectonic deformations forced the company to modify its exploration programme for the first time, in order to focus on zones where the probability of finding abundant mineralisation was higher.

Moreover, in two of its concessions the company carried out experimental field studies using the magnetotelluric method, with a total profiling length of 27 km. The results of magnetotelluric surveying were not accurate enough to trace the macro trends of copper mineralisation at depths exceeding 1500 metres. For this reason, the company decided to discontinue the use of this method.

4 Results of geochemical analyses

The analyses of archival core samples included a wide range of specialised examinations of organic matter. Their results show positive correlation between the occurrence of orebodies and pervasiveness of the alteration of organic matter in rocks hosting the ore (Oszczepalski and Speczik 2009, Zieliński et al. 2017). Oxidised rocks are depleted of organic carbon and exhibit a lower hydrogen index, while their vitrinite reflectance index, thermal maturity and oxygen index are elevated (Table 1) (Sawłowicz 1993; Speczik 1994). Moreover, dominant components of organic matter in copper-bearing shale include macerals from the liptinite group, with vitrinite and inertinite group macerals occurring in minor amounts (Speczik and Pütmann 1987).

Furthermore, Miedzi Copper Corp. performed organic matter decomposition tests on the collected core samples using the Rock-Eval pyrolysis. Results showed the presence of strong Rote Fäule in prognostic and prospective areas. High grade copper mineralisation is usually directly correlated with strong Rote Fäule zones (Oszczepalski and Speczik 2009), thus the identification of such alteration became a strong argument in favour of further exploration in selected areas.

Table 1. Differences in the parameters of organic matter between mineralised zones and oxidised zones of the Fore-Sudetic Monocline (after Sawłowicz 1993, Speczik 1994). TOC - total organic carbon, HC - hydrocarbons, Ph/ΣMePh – phenanthrene/total methylphenanthrene ratio, Vr - vitrinite reflectance.

Cu-bearing shales	Mineralised zones	Oxidised zones (RF)
TOC [%]	12.6	4.6
HC/TOC	0.015	0.004
Saturated HC/ aromatic HC	0.71	0.29
S in bitumines [%]	2.1	3.1
Ph/ΣMePh	0.9	2.2
Vr [%]	0.7	1.1
H/C in kerogen	0.89	0.44
O/C in kerogen	0.16	0.12

5 Drilling programme and its results

Based on the results of the above-mentioned analyses, more precise boundaries of prospective areas were established (Oszczepalski et al. 2016). Furthermore, Miedzi Copper Corp. amended some of its concessions before the initiation of drilling operations. The company decided to resign from areas where the base of Zechstein was particularly deep and initial investigation of mineralised intervals indicated low grades. Before the commencement of drilling, the only available data about Zechstein base in deep parts of the Fore-Sudetic Monocline originated from oil and gas wells.

Of the 32 holes drilled in the years 2013-2019, 24 produced positive results in terms of Cu-Ag grade. Moreover, all boreholes led to more precise identification of boundaries between major oxidised fields and reduced zones. After the initial phase of drilling, certain concessions were reduced in area in order to focus on the richest, the most prospective parts – the so-called “sweet spots”. Effectively, the operations continued in 6 most promising concessions (Nowa Sól, Wilcze, Zatonie, Jany, Mozów-1 and Sulmierzyce). As a result of its drilling operations, Miedzi Copper Corp. has discovered 3 stratiform Cu-Ag deposits in Poland – Nowa Sól, Mozów and Sulmierzyce, lying within the boundaries of all six aforementioned concessions.

6 Geology – new aspects

The drilling results indicate that the general ore distribution and zonation are similar to the Legnica-Głogów Copper District, with the ore-bearing zones being adjacent to oxidised fields. The biggest differences involve narrow zones of very intense mineralisation, as well as the fact that areas with elevated Pb-Zn content are more extensive. Furthermore, in numerous holes lead and zinc minerals occur at the same depths as copper and silver, instead of forming a separate layer above them like in the mining district. This is caused by the presence of two sources of mineralising fluids: the

Szprotawa and Wolsztyn elevations, which resulted in the mixing of brines and a more polymetallic nature of mineralisation. An example of this can be seen in Figure 1, which shows selected core samples from the Nowa Sól C14B hole, along with the results of chemical analyses of the whole ore-bearing interval.

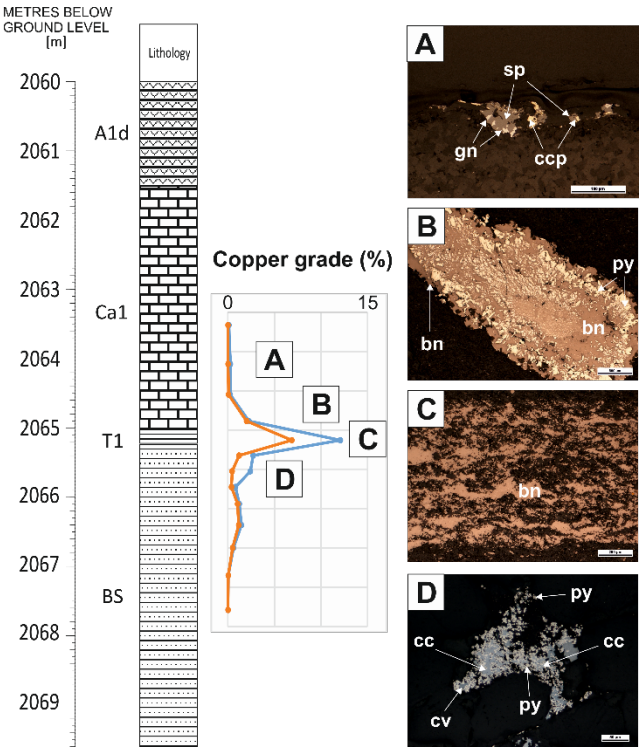

Figure 1. Example of Lower Zechstein profile from the Nowa Sól C14B borehole with results of chemical analyses and ore mineralogy. Orange line represents copper grade, blue line represents polymetallic copper equivalent grade (Cu+Ag+Pb+Zn) calculated using the formula of Zieliński and Wierchowiec (2018). Lithostratigraphic abbreviations: A1d – Lower Anhydrite; Ca1 – Zechstein Limestone; T1 – Copper-bearing shale (Kupferschiefer); BS – Weissliegend. Photomicrograph abbreviations: sp – sphalerite; gn – galena; ccp – chalcopyrite; py – pyrite; bn – bornite; cc – chalcocite; cv – covellite.

6.1 The Mozów deposit

The Mozów deposit is characterised by the deepest mineralised interval that occurs at the depth from 2100 to 2700 metres below ground level. The location of the deposit is shown in Figure 2A. Currently, the estimated resources are 4.4 million tonnes of Cu and 7.3 thousand tonnes of Ag in Polish category C_2 (an equivalent of indicated resources), with average thickness of 2.45 metres and average copper content amounting to 2.42%. Additional resources in category D_1 (inferred) are 8.4 million tonnes of Cu and 11.9 thousand tonnes of Ag. Despite the depth, according to a technical report prepared by Runge-Pincock-Minarco, mining operations in this deposit are economically justified. The estimated production costs are US $ 2705 per 1 tonne of copper with underground milling or US $ 2765 per 1 tonne with conventional milling (Goodell et al. 2017). All calculations for this and the following deposits are based on an expected average copper price of US $ 3 per 1 pound in a 10-year period.

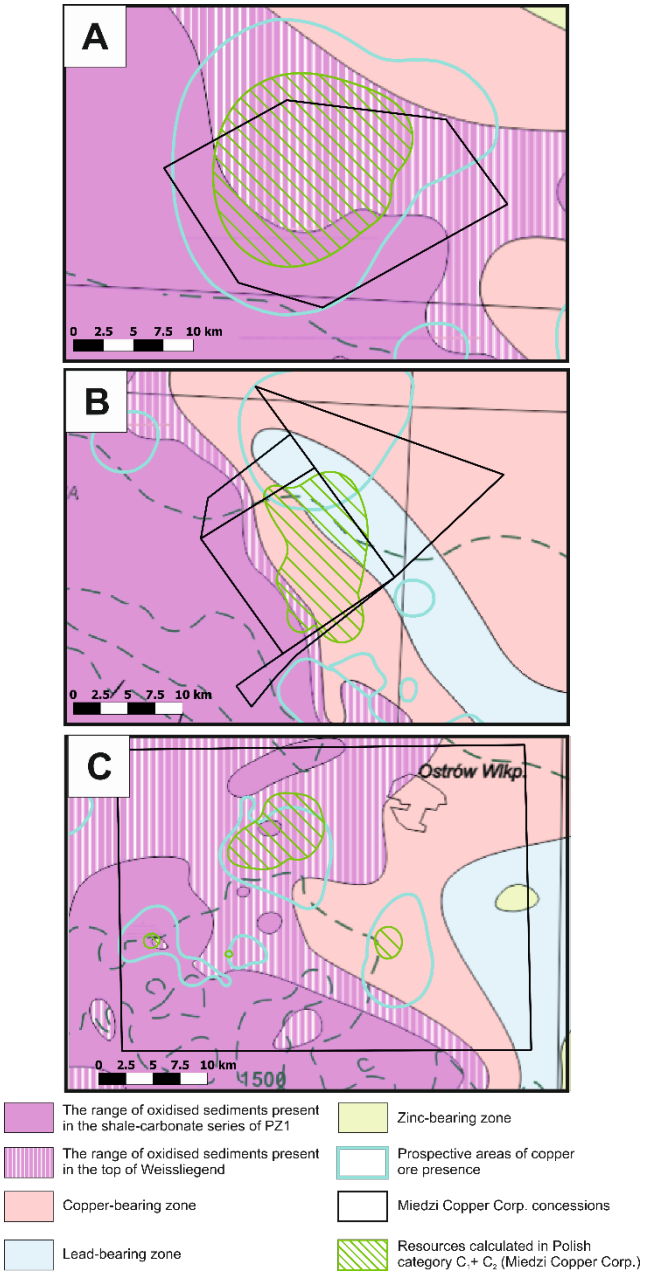

Figure 2. Miedzi Copper Corp.'s concessions and boundaries of resources calculated in Polish categories C_1+C_2. Geochemical zonation and prospective areas are based on Oszczepalski and Speczik (2011) and Oszczepalski et al. (2016).

6.2 The Nowa Sól deposit

The Nowa Sól deposit partially overlaps 4 concession areas: Nowa Sól, Jany, Zatonie and Wilcze (Figure 2A). The depth of the mineralised interval in that deposit varies from 1500 to 2400 metres below ground level. The demarcation of this deposit was a true greenfield discovery, as there had been no historical boreholes in the Nowa Sól concession, with no archival cores to examine before the initiation of Miedzi Copper Corp.'s

drilling programme. Currently, the estimated resources in categories C_1+C_2 (indicated and measured) are 7.0 million tonnes of Cu and 17.8 thousand tonnes of Ag, with average thickness of 3.40 meters and 1.40% of copper. Additional 4.5 million tonnes of Cu and 11.0 thousand tonnes of Ag are calculated in category D_1 (inferred). According to the technical report, mining operations in this area are also possible from an economic point of view. The estimated production costs are US $ 2670 per 1 tonne of Cu with underground milling or US $ 2698 per 1 tonne with conventional milling (Goodell et al. 2017). Geological documentation of the Nowa Sól deposit fulfilling the requirements of Polish law is in the final stage of preparation and it will be presented to the Minister of Environment in 2019. After the Minister's approval it will be possible to apply for a mining licence.

6.3 The Sulmierzyce deposit

The mineralised interval of the Sulmierzyce deposit lies between 1400 and 2000 metres below ground level. The location of the deposit is shown in Figure 2B. The current estimated resources in categories C_1+C_2 (indicated and measured) are 4.7 million tonnes of Cu and 10.5 thousand tonnes of Ag with average thickness of 1.87 metres and 2.93% of copper. Resources in category D_1 (inferred) are 5.4 million tonnes of Cu and 13.2 thousand tonnes of Ag. According to the technical report, future mining operations are also economically justified. The estimated production costs are US $ 2429 per 1 tonne of Cu (Bohnet 2017). Geological documentation of this deposit is also in preparation and it will be conveyed to the Minister of Environment in the middle of 2019.

7 Summary

Calculations have proved that mining operations in all deposits discovered by Miedzi Copper Corp. are economically profitable for the assumed average copper price of US $ 3 per 1 pound. Underground extraction should focus on copper ore of the best quality and highest grade. Currently available mining techniques are sufficiently developed to meet the challenge of building a deep copper and silver mine on discovered new Polish deposits of the Fore-Sudetic Monocline. The construction of mines in these areas is determined by the introduction of modern mining techniques of shaft sinking, waste management and air conditioning (Addison et al. 2012; Bohnet 2017; Goodell et al. 2017; Zieliński and Speczik 2017). Miedzi Copper Corp.'s drilling operations are currently continuing in the Nowa Sól area with the purpose of increasing the amount and accuracy of resources which will be disclosed in the annex to the geological documentation of this deposit.

References

Addison R, Bohnet E, Haptonstall J (2012) Conceptual Mine Planning for Underground Extraction of Polish Kupferschiefer Copper Deposits. Pincock, Allen & Holt for Miedzi Copper Corporation, Lakewood

Bellas I, Tassou SA (2005) Present and future applications of ice slurries. Int J Refrigeration 28:115-121

Bohnet E (2017) Technical Report on Miedzi Copper's Sulmierzyce Project, Poland

Goodell T, Jorgensen M, Bohnet E (2017) Technical Report of the Miedzi Copper Project, Poland

Oszczepalski S (1989) Kupferschiefer in southwestern Poland – sedimentary environments, metal zoning and ore controls. In: Boyle RW, Brown AC, Jowett EC, Kirkham R (ed) Sediment-hosted stratiform copper deposits. Geol Assoc Can Spec Paper 36:571-600

Oszczepalski S, Chmielewski A, Sowula W, Boratyn J, Pikuła K, Zieliński K (2012) Ocena możliwości występowania cechsztyńskiej mineralizacji Cu-Ag na obszarze województw lubuskiego i wielkopolskiego na podstawie archiwalnych materiałów wiertniczych, w tym wierceń naftowych. Polish Geological Institute, Warsaw

Oszczepalski S, Rydzewski A (1997) Metallogenic Atlas of the Zechstein Copper-bearing Series in Poland. Polish Geological Institute, Warsaw

Oszczepalski S, Speczik S (2009) Maturity assessment by Rock-Eval pyrolysis as an exploration tool, Kupferschiefer, Poland. In: WILLIAMS PJ et al (ed) Smart Science for Exploration and Mining. Proceedings of the Tenth Biennial SGA Meeting, Townsville 2009, pp 734-736

Oszczepalski S, Speczik S (2011) Copper and silver ores. In: Wołkowicz S, Smakowski T, Speczik S (ed) The balance of mineral resources deposits in Poland as of 31.12.2009. Polish Geological Institute, Warsaw, pp 76-93

Oszczepalski S, Speczik S, Małecka K, Chmielewski A (2016) Prospective copper resources in Poland. Gospod Surowcami Mineralnymi - Mineral Resources Management 32:5-30

Pieczonka J, Piestrzyński A, Lenik P, Czerw H (2007) Distribution of ore minerals in the copper deposit, Fore Sudetic Monocline. Biul Państw Inst Geol 423:95-108

Sawłowicz Z (1993) Organic matter and its significance for the genesis of the copper–bearing shales (Kupferschiefer) from the Fore–Sudetic monocline (Poland). In: Parnell J et al (ed) Bitumens in Ore Deposits. Springer–Verlag, Berlin, pp 431-446

Speczik S (1994) Kupferschiefer mineralization in the light of organic geochemistry and coal petrology studies. Geol Quart 38:639–650

Speczik S, Dziewińska L, Pepel A, Jóźwiak W (2012) Reprocessing of archival geophysical data as useful instrument in Cu-Ag deposit prospection of Fore-Sudetic Monocline. Biul Państw Inst Geol 452:257-286

Speczik S, Oszczepalski S, Chmielewski A (2013) Exploration and mining perspective of the Kupferschiefer series in SW Poland: digging deeper? Proceedings of the Twelfth Biennial SGA Meeting, Uppsala 2013, pp 687-690

Speczik S, Püttmann W (1987) Origin of Kupferschiefer mineralization as suggested by coal petrology and organic geochemical studies. Acta Geol Pol 37:167-187

Zieliński K, Speczik S (2017) Deep copper and silver deposits – a chance for Polish metal mining industry. Biul Państw Inst Geol 468:153-164

Zieliński K, Speczik S, Małecka K (2017) The strategy, instruments and results of deep copper and silver deposit exploration in the Fore-Sudetic Monocline. Zesz Nauk Inst Gosp Sur Min i En PAN 100:313-328

Zieliński K, Wierchowiec J (2018) The equivalent copper producibility of polymetallic Cu, Ag, Zn, Pb mineralisation in the Fore-Sudetic Monocline as illustrated by the "Sulmierzyce-Odolanów" prospective area. Zeszyty Naukowe IGSMiE PAN, 106: 257-274.